Histone variant H2B.Z acetylation is necessary for maintenance of *Toxoplasma gondii* biological fitness

Laura Vanagas[1], Daniela Muñoz[1], Constanza Cristaldi[1], Agustina Ganuza[1], Rosario Nájera[1], Mabel C. Bonardi[1], Valeria R. Turowski[2], Fanny Guzman[3], Bin Deng[4], Kami Kim[5], William J. Sullivan Jr.[6] and Sergio O. Angel[1]

[1]Laboratorio de Parasitología Molecular, INTECH, CONICET-UNSAM, Av. Intendente Marino Km. 8.2, C.C 164, (B7130IIWA), Chascomús, Prov. Buenos Aires, Argentina.

[2]Laboratorio de Bioquímica y Biología Celular de Parásitos, INTECH, CONICET-UNSAM, Av. Intendente Marino Km. 8.2, C.C 164, (B7130IIWA), Chascomús, Prov. Buenos Aires, Argentina.

[3]Núcleo de Biotecnología Curauma, Pontificia Universidad Católica de Valparaiso. Av. Universidad 330 Curauma, Valparaiso

[4]Department of Biology and VBRN, University of Vermont, Vermont, USA.

[5] Department of Internal Medicine, Morsani College of Medicine, University of South Florida, Tampa, FL 33612

[6] Department of Pharmacology and Toxicology, Indiana School of Medicine, Indianapolis, Indiana 46202, USA

Corresponding author: Sergio O. Angel. Laboratorio de Parasitología Molecular, IIB-INTECH, CONICET-UNSAM, Av. Intendente Marino Km. 8.2, C.C 164, (B7130IIWA), Chascomús, Prov. Buenos Aires, Argentina. Tel.: +542241424303

E-mail address: sangel@intech.gov.ar (SO Angel)

Abstract

Through regulation of DNA packaging, histone proteins are fundamental to a wide array of biological processes. A variety of post-translational modifications (PTMs), including acetylation, constitute a proposed histone code that is interpreted by "reader" proteins to modulate chromatin structure. Canonical histones can be replaced with variant versions that add an additional layer of regulatory complexity. The protozoan parasite *Toxoplasma gondii* is unique among eukaryotes in possessing a novel variant of H2B designated H2B.Z. The combination of PTMs and the use of histone variants is important for gene regulation in *T. gondii,* offering new targets for drug development. In this work, *T. gondii* parasites were generated in which the 5 N-terminal acetylatable lysines in H2B.Z were mutated to either alanine (c-Myc-A) or arginine (c-Myc-R). c-Myc-A mutant only displayed a mild effect in its ability to kill mice. c-Myc-R mutant presented an impaired ability to grow and an increase in differentiation to latent bradyzoites. This mutant line was also more sensitive to DNA damage, displayed no virulence in mice, and provided protective immunity against future infection. While nucleosome composition was unaltered, key genes were abnormally expressed during *in vitro* bradyzoite differentiation. Our results show that the N-terminal positive charge patch of H2B.Z is important for these procceses. Pull down assays with acetylated N-terminal H2B.Z peptide and unacetylated one retrieved common and differential interactors. Acetylated peptide pulled down proteins associated with chromosome maintenance/segregation and cell cycle, opening the question of a possible link between H2B.Z acetylation status and mitosis.

Key words: *Positive charge patch – cell cycle – differentiation – virulence – mitosis*

45 # Introduction

46 Histones proteins function to form nucleosomes that regulate packaging of DNA, thereby affecting
47 DNA transcription, replication, and repair. In addition to the four canonical histones (H2A, H2B, H3 and H4),
48 variant histones exist that can be substituted into the nucleosome, affecting its properties. Canonical and
49 variant histones are also subject to a wide array of post-translational modifications (PTMs) that can alter
50 the nucleosome or recruit chromatin remodeling machinery. The combination of PTMs and exchange of
51 histone variants is believed to be important for gene regulation in the protozoan parasite *Toxoplasma*
52 *gondii,* offering new targets for drug development [1-3].

53 *T. gondii* is a member of phylum Apicomplexa and infects between 10-90% of the population
54 depending on the country [4], presumably influenced by dietary habits and environmental conditions [5].
55 *T. gondii* converts from rapidly growing tachyzoites, which cause acute infection, to slow or non-growing
56 bradyzoites, which cause chronic infection and typically reside in the brain [6]. Although *T. gondii* infection
57 is asymptomatic in healthy people, untreated clinical toxoplasmosis can be lethal in immunocompromised
58 individuals such as transplant or HIV patients, and can produce severe disease during congenital infection,
59 especially in early stages of development [7, 8]. Chronic toxoplasmosis has also been linked to brain tumor
60 predisposition, attention-deficit/hyperactivity disorder, obsessive-compulsive disorder and schizophrenia
61 [9-13].

62 The *T. gondii* life cycle is comprised of sexual and asexual stages. While sexual replication takes
63 place only in felids, *T. gondii* is able to replicate asexually as tachyzoites in any nucleated cell in any warm-
64 blooded vertebrate. Following infection, tachyzoites convert into bradyzoites, which are house in tissue
65 cysts that are impervious to immunity and current drug treatments. Recently, a myb-like transcription
66 factor (BFD1) was described to be necessary and sufficient to induce bradyzoite differentiation [14]. How
67 BFD1 is recruited to stage-specific promoters remains to be determined, but likely involves interplay with

68 chromatin remodelers and epigenetic processes that include histone PTMs and/or variant histone exchange
69 [15]. In support of this idea, treatment of tachyzoites with inhibitors of histone deacetylase 3 (HDAC3)
70 initiates bradyzoite differentiation [16]. The roles of histone variants in *T. gondii* remain poorly understood.

71 *T. gondii* expresses histone variants that we have previously shown mark functional regions of the
72 genome [17]. H2A.Z is a ubiquitous variant that has been implicated in both transcriptional activation and
73 gene silencing in eukaryotes, and in fine regulation of important processes as DNA damage repair [18-20],
74 which is also present in *T. gondii* [21]. Unlike H2A.Z, only specialized isoforms of the H2B histone family
75 have been described in nature, except for apicomplexan parasites [22-25] and trypanosomatids [26], in
76 which a H2B.Z and a H2Bv variants, were identified, respectively.

77 Histones H2A.Z and H2B.Z form a dimer that localizes with the transcriptional activation mark
78 H3K4me3 in promoter/transcriptional start site (TSS) regions surrounding the nucleosome-free region
79 upstream of the transcription start site [17]. In addition, H2B.Z and H2A.Z histones localize to the gene
80 bodies of silent genes, including repressed stage-specific genes, suggesting a role in the regulation of stage
81 transitions. In *T. gondii*, both H2A.Z (TGGT1_300200) and H2B.Z (TGGT1_209910) are essential during the
82 lytic cycle with CRISPR fitness scores of -5.08 and -4.05, respectively [27]. By mass spectrometry, both
83 histone variants were found to be hyperacetylated at the N-terminal domain, whereas few or no acetylation
84 marks were identified on canonical H2A, H2B and H2A.X [28]. *T. gondii* H2B.Z was shown to be acetylated
85 at 5 lysine residues in its N-terminal tail. The H2A.Z N-terminal tail has 10 acetylatable lysines, in which
86 lysine 18 can also be methylated [28]. H2A.Z N-terminal tail acetylation has been widely shown to be a
87 hallmark for active chromatin whereas N-terminal methylation is associated with gene silencing [29-32],
88 suggesting it is essential for changes in gene expression during cell differentiation [33-37]. While the role
89 of N-terminal lysine acetylation in H2B.Z has not yet been studied, N-terminal acetylated canonical H2B is
90 associated with some, but not all, active genes in vertebrates [38]. Interestingly, H2A.Z in most eukaryotes
91 only bears 4-5 acetylatable lysine residues in the N-terminus, while in protists like *T. gondii, Plasmodium* or

92 *Tetrahymena termophila,* this number is considerably higher (between 5 and 16). Moreover, the presence
93 of a *T. gondii* double variant nucleosome that altogether carries 15 acetylatable lysines that could be
94 regulated is highly intriguing.

95 In the present work we studied the role of the five *T. gondii* H2B.Z N-terminal tail lysines, using a
96 mutagenesis strategy; we also pursued a gene knockout strategy for H2B.Z. In an RH strain background, we
97 generated *T. gondii* that possess mutated versions of H2B.Z: c-Myc-R, in which the five N-terminal
98 acetylatable lysines were replaced by arginines, and c-Myc-A, in which they were replaced by alanines.
99 These lines were analyzed for their ability to grow *in vitro*, differentiate to bradyzoites *in vitro* and produce
100 virulence in mice. In addition, expression of key genes was studied, as well as nucleosome composition and
101 DNA damage sensitivity. Our results suggest that regulation of the N-terminal positive charge patch by
102 lysine acetylation, rather than the histone code, is essential for the aforementioned biological processes.
103 We have also found some differential interactors for an acetylated N-terminal H2B.Z peptide, compared to
104 a unacetylated one, opening new questions on the function of this modification and this histone variant.
105 The implications of these data on the putative role of H2B.Z is discussed.

106

107 # Results

108 **Sequence alignment of Apicomplexa H2B.Z N-tail**

109 H2B.Z is a variant histone of the H2B family that appears early in the phylum Apicomplexa.
110 Previously, it was observed that *T. gondii* and *Plasmodium falciparum* H2B.Z N-terminal tails contain five
111 acetylated lysines (K4,K9,K13,K14 and K18) [28, 39, 40]. The conservation of the five acetylatable lysines is
112 clear from the alignment of H2B.Z N-terminal tail sequences from different Apicomplexa (Fig. 1A). This
113 profuse number of modifications in the N-terminal tail, concomitant with the nucleosome partner, H2A.Z,

114 in which several acetylatable lysines are present, make this double variant nucleosome a likely feature for
115 chromatin modification relevant to gene expression, replication and/or DNA damage responses.

116

117 **Overexpression of tagged wild type and mutant versions of H2B.Z and Knock out of endogenous *H2B.Z***

118 Attempts to obtain a mutant cell line by deletion of the *h2b.z* gene were unsuccessful (data not
119 shown). The failure to obtain an H2B.Z. knockout is consistent with its CRISPR fitness score of -4.05, strongly
120 suggesting it is essential [27] (ToxoDB, TGGT1_209910).

121 Given the high number of modifiable lysines in the H2B.Z variant unique to apicomplexan parasites,
122 we analyzed their role by using an over-expression strategy of myc-tagged wild-type or mutant forms. We
123 generated parasites over-expressing wild-type H2B.Z (c-Myc-WT-OE) or a mutated form in which all the
124 acetylatable lysines in the N-terminal tail were changed to alanine, which mimics how acetylation ablates the
125 positive charge of the lysine residues. We also over-expressed a mutated version in which the lysines were
126 replaced with arginines, which would generate a constitutive positive charge patch but no longer support
127 acetylation (Fig. 1B). Neither mutant form would be acetylated in this region, therefore would be incapable
128 of interacting with bromodomain containing proteins. Correct localization of each c-Myc-H2B.Z protein was
129 checked by immunofluorescence (IFA) (Fig. S1A) and by western blotting, observing two bands in every over-
130 expressing line (Fig. S1B). To note, c-Myc-WT-OE was already used in a ChIP seq screen, showing the same
131 genomic localization as endogenous H2B.Z when the experiments were performed using α-H2B.Z antibody
132 [17].

133 After that, endogenous *H2B.Z* gene was deleted by using CRISPR methodology in the previously
134 generated *T. gondii* lines overexpressing mutant H2B.Z versions (Fig 2A). We took advantage of the number
135 of mutations in the N-terminal tail of the tagged version to design sgRNA specific for endogenous *H2B.Z* gene.
136 We obtained *T. gondii* RH lines only expressing c-Myc-tagged H2B.Z with N-terminal mutations, which were

137 named c-Myc-A and c-Myc-R (Fig. 2A-C, Fig. S1C-D). Each form of c-Myc H2B.Z in these parasites localized
138 properly to the nucleus (Fig. 2B). In both CRISPR manipulated clones, a single band corresponding to c-Myc-
139 tagged H2B.Z can be observed by western blot with anti-H2B.Z and anti-c-Myc antibodies (Fig. 2C).
140 Quantification of the band corresponding to c-Myc H2B.Z relativized to Sag1 as a charge control, was 1.43 ±
141 0.77 and 1.65 ± 0.82 for c-Myc-R and c-Myc-A, respectively, indicating comparable levels of expression
142 between both mutants.

143

144 ***In vitro* growth analysis in c-Myc-R and c-Myc-A *T. gondii* lines**

145 We used a competitive growth assay to determine differences in parasite growth between parental
146 wild-type and mutant parasites (c-Myc-A and c-Myc-R) obtained, which could be distinguished by the c-Myc
147 tag. Approximately equal amounts of c-Myc positive and c-Myc negative (parental) tachyzoites were mixed
148 and allowed to invade hTert cells, which were analyzed by IFA on different days post-infection. While the c-
149 Myc-A parasites showed no change in growth relative to the parental line over time, the c-Myc-R line showed
150 a marked growth deficiency compared to the parental line (Fig. 3A). As arginines conserve the positive charge
151 but cannot be acetylated, these results indicate that the constitutive positive charge patch on the H2B.Z N-
152 terminal tail, but not the lack of acetylation, impairs tachyzoite growth *in vitro*. Therefore, wild-type *T. gondii*
153 must regulate the charge patch on H2B.Z N-terminal tail by PTMs such as acetylation for normal growth.

154

155 ***In vitro* differentiation analysis in c-Myc-R and c-Myc-A *T. gondii* lines**

156 We next studied the effect of the mutant H2B.Z variants on *in vitro* tachyzoite to bradyzoite
157 differentiation using alkaline stress to trigger stage conversion and *Dolichos biflorus* lectin (DBL) to monitor
158 tissue cyst wall formation. Strikingly, we found that c-Myc-R, but not c-Myc-A, showed an increase in DBL-

159 positive vacuoles compared to the wild-type control (Fig. 3B), suggesting that the impossibility to regulate
160 the presence of a positive charge patch in the H2B.Z N-terminal tail promotes an *in vitro* differentiation.

161 We also checked whether key stage-specific genes were altered in parasites expressing mutant
162 H2B.Z. We obtained RNA from freshly lysed tachyzoites, early bradyzoites (48 hours post-differentiation),
163 and late bradyzoites (96 hours post-differentiation) of the parental RH strain and c-Myc-A or c-Myc-R
164 parasites. We analyzed the expression of *Sag1* (tachyzoite), *Bag1* (early bradyzoite), *LDH2* (early bradyzoite),
165 *AP2IX-9* (mature bradyzoites) [41], *AP2 IV-3* (in which expression is maximal at 48h post- differentiation,
166 decreasing in mature bradyzoites) [42] and *BFD1* [14] mRNA by RT-qPCR. Actin and Tubulin were used as
167 housekeeping genes, and data were normalized to actin. The amount of expression relative to tachyzoite in
168 each parasite line is plotted, showing a trend of expression in c-Myc-R similar to what would be expected for
169 a cystogenic strain with the treatment, and different from RH expression profile (Fig. 3C). Also, the expression
170 of *BFD1* showed an increase in c-Myc-R, compared to RH (Fig. 3C). Notably, the expression profile of BFD1 in
171 RH type I strain has not been published to date. These results are consistent with the heightened bradyzoite
172 differentiation rate seen in c-Myc-R parasites.

173

174 **Sensitivity to DNA damaging agents in c-Myc-A and c-Myc-R lines**

175 In other species, H2A.Z has been linked to double strand break repair driven by the non-homologous
176 end joining (NHEJ) pathway [20, 43, 44]. Consequently, H2A.Z is associated as a responder to HU or MMS
177 genotoxic effects [44]. We have previously characterized the anti-*T.gondii* effect of MMS, HU, and
178 campothecin [45]. Topotecan is a genotoxic drug analog to campthotecin that produces fork collapse, and
179 ulterior DNA double strand break repaired by HRR [46].

180 Given the roles of histone variants in DNA repair, we analyzed c-Myc-A and c-Myc-R parasites for
181 sensitivity to topotecan at its IC_{50} value (20 μM) and MMS (50 μM) using the competitive growth assay. We

182 observed a significative decrease in growth compared to the parental after treatment only with MMS for c-
183 Myc-R tachyzoites (Fig. 4A). By contrast, topotecan did not produce a significant defect in growth, although
184 c-Myc-R seems to be more sensitive (Fig. 4A). In addition, treatment with MMS produced a disorganization
185 of vacuoles, rounded shapes and a loss of genetic material in both mutants as well as parental (Fig. 4B). *T.*
186 *gondii* normally presents a synchronic replication in the parasitophorous vacuole (PV). As a result, PVs usually
187 show 2, 4, 8, 16 and so on, tachyzoites (Tz) per PV. Treatment with MMS and Topotecan also caused a loss
188 of synchronization, with an altered number of Tz per PV, which was also counted as "anomalous vacuole".
189 Anomalous vacuoles and loss of genetic material were also observed with topotecan treatment (Fig. 4B).
190 However, quantification showed that anomalous PV are significatively more abundant in c-Myc-R than
191 parental and c-Myc-A, with both drugs tested (Fig. 4C). Taken together, the constitutive positive charge patch
192 generated in the c-Myc-R parasites alter the DNA damage response after MMS treatment, suggesting that
193 acetylation status of H2B.Z N-terminal tail is likely to be modulated for proper DNA repair.

194

195 ***In vivo* analysis in c-Myc-R and c-Myc-A *T. gondii* lines**

196 Proper gene regulation is required for tachyzoite propagation in different tissue environments and
197 differentiation *in vivo*. Progression of tachyzoite infection of these mutants was analyzed in C57BL/6 mice by
198 inoculating 100 tachyzoites per *T. gondii* line. As expected, parental parasites displayed high virulence, killing
199 mice within 7 days (Fig. 5A). c-Myc-A tachyzoites were also lethal to mice, but with a delay in the time of
200 death (Fig. 5A). According to Mantel-Cox and Gehan-Breslow-Wilcoxon tests, the survival curves are
201 significantly different ($p>0.0001$), suggesting that acetylation of at least some of the 5 N-terminal tail lysines
202 is relevant for parasite progression *in vivo*.

203 In contrast, c-Myc-R and Me49 infected mice, as well as non-infected (PBS group) survived until
204 sacrifice on day 30-35 (Fig. 5A). c-Myc-WT-OE was used a control that the tagged version is not responsible

205 *per se* of any affect observed. *T. gondii* line expressing both endogenous H2B.Z and c-Myc-H2B.Z-R (c-Myc-R-
206 OE) previous to CRISPR procedure, were as lethal as the parental line (data not shown), suggesting that the
207 randomly integrated ptub-*H2B.Z-R* gene is not responsible for the loss of virulence. Infection with 1,000 and
208 10,000 c-Myc-R tachyzoites were also nonlethal to mice (Fig S2A).

209 To confirm acute infection took place, hematoxylin and IFA staining of the peritoneal fluids at day 4
210 post-infection were performed (Fig. 5B). Intraperitoneal tachyzoites could be detected only with parental
211 and c-Myc-A *T. gondii* lines infections, but not with c-Myc-R parasites (Fig. 5B). Surviving animals (c-Myc-R
212 and Me49 *T. gondii* lines) were analyzed to detect antibodies against *T. gondii*. An increase in total IgG in
213 mice infected with c-Myc-R tachyzoites was observed, comparable to Me49, which indicated that an initial
214 infection had taken place (Fig. 5C, Fig. S2B). The analysis of IgG subtypes showed a Th1-like humoral response
215 in both cases, associated to IgG2a and higher for IgG2b (normal for C57/BL6 mice), typical for an intracellular
216 parasite infection (Fig. 5C, Fig. S2B). Following sacrifice, brains of surviving mice were processed for cyst
217 detection by direct observation with optical microscopy and DBL staining. Tissue cysts were observed in
218 brains of mice infected with Me49 strain, but not in those infected with c-Myc-R parasites (data not shown).

219 To determine if infection with c-Myc-R parasites elicits an adequate immune response, mice
220 previously infected with 1,000 c-Myc-R tachyzoites were reinfected with 100 tachyzoites of the highly virulent
221 RH parental line. c-Myc-R infected mice survived until sacrifice, while all mice in the control group died at day
222 38 (day 8 after re-infection) (Fig. 5D). These results suggest that c-Myc-R tachyzoites must have been capable
223 of invading cells and producing a stimulation of the cellular immune response adequate to control a challenge
224 infection.

225

226 **H2B.Z acetylation status is involved in regulation of ROP proteins expression**

227 The ability of the c-Myc-R line to establish a protective immune response suggest these parasites can
228 invade the host cells but are efficiently controlled by the immune system. Among the *T. gondii* virulence
229 proteins that exert protection from PV establishment are the polymorphic rhoptry proteins Rop5 and Rop18,
230 which disrupt the γIFN-inducible IGR pathway [47-51]. Here, we used antibodies against *T. gondii* Rop5
231 (TGGT1_411430) and Rop18 (TGGT1_205250) recombinant proteins for western blot analysis. Rop5 was
232 present in parental, c-Myc-A, and c-Myc-R parasites, whereas Rop18 only in the parental line (Fig. 6A).
233 However, quantification of the band intensities showed a significative decrease in Rop5 abundance in c-Myc-
234 R parasites and a lack of Rop18 protein in both c-Myc-A and c-Myc-R (Fig. 6B and Fig. S3A). To test whether
235 the absence of Rop18 was a consequence of the insertion of the H2B.Z construction in that locus, we
236 performed the same experiment using the over-expressing tachyzoites obtained prior to CRISPR
237 manipulation. As shown in Fig.S3 (B, C) both Rop5 and Rop18 are detectable in every clone similar to parental.
238 Co-localization analysis showed a correct localization of Rop5 in all *T. gondii* lines whereas Rop18 could only
239 be detected in the parental line (Fig. 6C). Of note, we also detected a decrease in the fluorescence intensity
240 of Rop5 in c-Myc-R parasites (Fig. 6D). RT-PCR analysis indicated that both genes were expressed in every *T.*
241 *gondii* line (Fig. S3D), suggesting that alteration of Rop5 and Rop18 expression in the c-Myc-R line is likely at
242 the post-transcriptional level.

243

244 **Double variant nucleosome and transcription is not altered in *T. gondii* mutant lines in normal conditions**

245 Since H2BZ is part of the double variant nucleosome with H2AZ, which is in the promoter region of
246 active genes, it was expected that expression alterations would occur at the transcriptional level rather than
247 post-trancriptionally. To determine if the observations for Rop5 and Rop18 were a specific situation, we
248 looked closer at the role of H2B.Z in transcription. We first analyzed the double variant (H2A.Z/H2B.Z)
249 formation in both mutant lines by co-immunoprecipitation (co-IP) assays by using commercial anti-c-Myc

250 agarose. Mononucleosomes of c-Myc-A and c-Myc-R lines were obtained after MNAse digestion before co-
251 IP (Fig. 7A). In figure 7B it can be observed that both c-Myc-A and c-Myc-R H2B.Z interact with H2A.Z,
252 confirming the assembly of the double variant nucleosome already found in *T. gondii*. We also decided to
253 study the interaction of the double variant nucleosome with acetylated H3, a known mark of active
254 chromatin. Both c-Myc-A and c-Myc-R H2B.Z interacted with this acetylated histone, which indicates that lack
255 of acetylation of H2B.Z does not alter this PTM crosstalk (Fig. 7B and Fig. S4). Quantification of the IP band
256 intensities relative to the respective input band showed that both *T. gondii* lines exhibit similar interaction
257 levels with H2A.Z and acetylated H3 (Fig. 7C). These data indicate that transcriptional expression was not
258 altered in c-Myc-R parasites with the double variant nucleosome remaining functional.

259 We next decided to explore if transcription was altered in tachyzoites of the mutant lines. We
260 analyzed expression of *Sag1* (tachyzoite), *tubulin* (constitutive), *Bag1* and *LDH2* (bradyzoite) and *BFD1*
261 (master differentiation factor). Only BFD1 expression was statistically higher in c-Myc-R that in the parental
262 or c-Myc-A (Fig. 7D), consistent with our observation that c-Myc-R parasites are more prone to differentiate
263 into bradyzoites.

264

265 **Chromatin compaction does not explain differences observed in *T. gondii* mutant lines**

266 The positive charge patch on H2B.Z could be associated with a more compact chromatin structure.
267 To analyze chromatin compaction, we measured the size of the nuclei of these lines compared to the parental
268 in IFAs stained with α-H2B.Z antibody. As shown in Fig. 7E, nuclei sizes are significantly smaller that the
269 parental in c-Myc-R parasites in accordance with the hypothesis. However, this significant difference is also
270 seen in c-Myc-A tachyzoites, indicating that the inability of this histone to be post-translationally modified is
271 enough to lead to this state. The sizes of c-Myc-WT-OE parasite nuclei were similar to parental nuclei,

272 suggesting that the c-Myc tag is not responsible for the effect observed (Fig. 7E). Taken together, acetylation
273 of the H2B.Z N-terminal tail is required for proper control of DNA compaction status.

274

275 **H2B.Z interacting proteins**

276 While results largely implicate the positive charge patch of H2B.Z N-terminal tail as responsible for the
277 observed phenotypes, a role for acetylation cannot be ruled out. Acetylation may explain why the c-Myc A
278 line showed a mild defect in virulence *in vivo* and defects in chromatin compaction. These defects could be
279 associated with the interaction with acetylation "reader" proteins. We therefore examined if there are
280 differential proteins interacting with H2B.Z N-terminal region depending on its acetylation state. We
281 designed two peptides, one containing two acetylated lysines (K14 and K18) and the other unacetylated;
282 both peptides contained a biotin tag towards the C-terminal end (Fig. 8). Peptide design was performed
283 according to Wysocka 2006 [52]. In this work, it was recommended to perform the synthesis of peptides
284 about 20 amino acids long, with biotin conjugated through a linker on the C-terminus for N-terminal histone
285 peptides, and with the modification positioned close to the center of the peptide. In addition, two
286 consecutive modifications were not recommended, explaining our choice of K14 and K18.

287 We used extracellular tachyzoites (RH) to perform the pull-down assays. After resolving on SDS-
288 PAGE, samples were analyzed by mass spectrometry. We detected a total of 48 interactors, 18 exclusive of
289 non-acetylated oligo, 17 exclusive of acetylated oligo and 14 present in both (Table S1). While many
290 interactors have nuclear localization, other localizations were detected, and many typical contaminants (e.g.
291 ribosomal subunits). Among the nuclear proteins, we can select a few that can be interacting with the H2B.Z
292 N-terminal tail independent of acetylation status; among them, GCN5-A, histone H4 and a PHD protein (Fig.
293 8). Interestingly, only three nuclear proteins were differentially pulled down at high score or with strong
294 evidence (2 independent pull downs), one of them TGME49_262620, a RRM protein (unacetylated peptide),

295 H3.3 and a putative CDK protein (both with the acetylated peptide). Considering the nuclear genes that only
296 appeared in 1 pull down, the acetylated peptide retrieved only genes that code for proteins associated with
297 the maintenance and segregation of chromosomes during the cell cycle, as peptidase c50 (TGME49_262825),
298 RecF/RecN/SMC N terminal domain-containing protein (TGME49_231170) and meiotic recombination
299 protein DMC1 family (TGME49_216400) (Table S1). Among the retrieved peptides in both acetylated and
300 non-acetylated pull-downs, we also detected acetyl-CoA carboxylase ACC1 (TGME49_221320) (Fig. 8 and
301 Table S1). It is interesting to observe that an apicoplast protein displayed a significant number of peptides,
302 indicative of a consistent interaction. We discuss the implications of these findings in the next section.

303

304

305 **Discussion**

306 In *T. gondii* gene expression is associated to the cell cycle, lytic cycle and differentiation [15, 53-58].
307 In addition to gene expression, the presence of histone variants as well as the turnover of PTMs on histones
308 are also associated to chromosomal organization, DNA repair or DNA replication [59]. The Apicomplexa
309 H2A.Z/H2B.Z double variant histone nucleosome is unique and is extensively modified by PTMs including N-
310 terminal tail acetylation. *T. gondii* epigenome has been studied, and it has been observed that this parasite
311 uses a set of different histone modifications as a complex set of tools to control its gene expression [60].
312 Acetylation and methylation are associated to opposite impacts in gene expression, the first favoring
313 expression, while the second is often a repressive mark. As an example, acetylation of lysine 31 on histone
314 H4 (H4K31) was associated to the promoter of a nearby active gene, while in the core body of these genes
315 H4K31me1 was detected [59]. Until now, the role of PTMs in *T. gondii* H2BZ has not been studied. However,
316 *T. gondii* H2B.Z/H2A.Z double variant nucleosomes were found in the promoter of active genes and in the
317 gene body of inactive genes [17]. This change in genomic location could be regulated by the different PTMs

318 of H2B.Z and/or H2A.Z. The present work is the first attempt to decipher the role of the N-terminal
319 acetylation of H2B.Z.

320 According to the results obtained in this work, the presence of a constitutive positive charge patch
321 in the N-terminal tail of the histone (c-Myc-R mutant) causes an increase in differentiation, a decrease in
322 growth, and an impaired DNA damage response *in vitro*. On the other hand, virulence was severely affected
323 *in vivo* indicating some sort of regulation at least in those processes for this H2B.Z PTM. Those effects were
324 not observed when lysine was replaced by alanine, an uncharged amino acid that mimics acetylated lysine,
325 except a mild effect on virulence *in vivo*. While these results argue in favor of control by the positive charge
326 patch as a crucial event in *T. gondii* tachyzoite, a minor or fine role supported by acetylation marks on the N-
327 terminal tail of H2B.Z cannot be ruled out. For *T. termophila* when engineering a constitutively positive
328 charge patch on H2A.Z, this was highly toxic, suggesting that its regulation has an essential function [61].
329 Moreover, the presence of a single acetylation site in this region was sufficient to avoid the toxic effect of
330 the positive charge patch [61, 62]. In our case, some phenotypical alterations were observed *in vitro*, but the
331 *T. gondii* c-Myc-R tachyzoites were viable except during mouse infection. This indicates that at least *in vitro*,
332 if there is a toxicity due to the constitutive positive charge patch of H2B.Z, it could be partly compensated by
333 H2A.Z, which presents 10 acetylatable lysines [28]. Together, H2A.Z/H2B.Z, would represent a "combined N-
334 terminal tail" of 15 lysines. Studies involving the role of acetylation on H2A.Z N-terminal tail of *T. gondii* are
335 needed to understand this.

336 An interesting aspect is that the *T. gondii* c-Myc-R line can grow responding to DNA damage *in vitro*,
337 with significant but surmountable defect. This would indicate a role in DNA damage repair for this histone
338 variant in *T.gondii*, with acetylation as a central player. However, this sensitivity was only significant for c-
339 Myc-R tachyzoites, arguing once again in favor of the positive charge patch toxicity hypothesis in this mutant.
340 Since H2B.Z does not exist in nature beyond Apicomplexa, we can only infer the putative role of this variant
341 histone being part of H2A.Z/H2B.Z nucleosome. The participation of H2A.Z in DNA damage repair pathways

342 has been studied in mammals and yeast [20, 43, 44]. More experiments should be conducted to analyze more
343 deeply the role of H2B.Z in DNA damage response.

344 However, the contributions of effects observed *in vitro* are less difficult to ascertain in the *in vivo*
345 model. Clearly c-Myc-R line is capable of invasion, generating an adequate immune response, but it is quickly
346 neutralized during the infective process. This suggests that the tachyzoite is exposed *in vivo* to stronger
347 environmental pressures than those observed *in vitro*. These pressures would include adaptation to new
348 environments, including different cell types and organs, which may present differences in metabolism,
349 nutrient availability, or immune responses. Under these conditions, where the tachyzoite must respond
350 quickly, fine reprograming of gene expression and modifications in metabolic pathways would be required
351 and the impossibility of modulating the positive charge patch of H2B.Z could hamper the ability of parasites
352 to adapt to changing environments *in vivo*.

353 A possible explanation for the changes provoked by the positive charges in the N-tail could be a
354 chromatin compaction due to interaction with the negative charges in DNA. Genome size expansion in
355 eukaryote evolution has led to an increase in histone H2A N-terminal tail arginines. Arginine-rich histones
356 bind more tightly to DNA, compacting chromatin and, in some cases, the nuclei are also smaller [63].
357 However, in this work we showed that nuclei size was smaller in both clones compared to parental and to c-
358 Myc-WT-OE tachyzoites, indicating that the charges in the N-terminal tail are not responsible for chromatin
359 compaction. Chromatin compaction has also been described to be regulated by linker histone H1, that
360 stabilizes the nucleosome structure. A candidate H1 has been recently identified in *T. gondii*, and interaction
361 of H1 with H2B.Z was observed [64]. The acetylation status of H2B.Z may be important for this interaction,
362 leading to a more compact chromatin in both alanine and arginine mutants because of linker histone H1.
363 Further experiments are needed to test this hypothesis.

364 It could be expected that the phenotypic alterations are given by defects in the formation of the
365 nucleosome with an impact on the expression of the genes. In our analysis, both situations are not altered.
366 Although a massive analysis of gene expression is necessary to detect specific changes, part of the study
367 shows that the expression of Rop5 and Rop18 does not occur at the transcriptional level, but rather post-
368 transcriptionally, affecting their translation. This regulation could be given by the presence of non-coding
369 RNAs (ncRNAs) and there is increasing evidence for a significant role for pos-transcriptional mechanisms [65,
370 66]. Future studies should take this possibility into account, considering a possible role of H2B.Z acetylation,
371 to analyze ncRNAs expression in *T. gondii*. With the results shown in this work it is only possible to correlate
372 the decrease in one of the more virulent isoforms of Rop5 together with the absence of Rop18 protein to the
373 loss of virulence of c-Myc-R mutant, although it cannot be ruled out that other virulence factors could be
374 altered in these parasites. On the other hand, the absence of Rop18 protein in c-Myc-A correlates with the
375 significative delay in mice death with c-Myc-A tachyzoites infection as reported by Resse et al [49].

376 Although we could not detect significative changes in most of the genes analyzed by RT-qPCR in
377 normal conditions for tachyzoites, *BFD1* was significatively higher in c-Myc-R. Interestingly, we observe a
378 higher differentiation rate *in vitro* for these parasites. The differentiation process of c-Myc-R under alkaline
379 stress was also accompanied by the expression of bradyzoite-specific genes. It is important to note that the
380 expression of the BFD1 gene is post-transcriptionally regulated [14]. Therefore, the increase in transcription
381 *per se* is not enough to induce differentiation, but the higher levels of BFD1 mRNA could favor differentiation
382 under alkaline stress. There is also another possibility of inducing differentiation based on epigenetic
383 regulation. HDACi FR235222 treatment was shown to favor acetylation of H4K31ac in bradyzoite gene
384 promoters, promoting transcription of bradyzoite genes and therefore, bradyzoite development [59]. The
385 fact that we only observe a mis-regulation in gene expression for c-Myc-R could be related to the constitutive
386 positive charge patch generated in this mutant. This could imply that the lack in modulation the positive

387 charges on H2B.Z could alter the correct role of this variant histone in the regulation of gene expression,
388 under alkaline stress.

389 The positive charge patch seems to be responsible for most of the differences shown in this work.
390 However, c-Myc-A mutant could be mimicking a situation where all H2B.Z N-terminal lysines were neutralized
391 by a PTM such as acetylation. This situation could be the most physiological one for the parasites, and why
392 c-Myc-A tachyzoites have a similar phenotype as the parental. The results obtained in the pull-down
393 experiments may be in consonance. While acetylated and unacetylated peptides pull-downs share 3 nuclear
394 proteins: GCN5A, PHD and clathrin, unacetylated peptide recognized one protein specifically, a RNA
395 recognition motif (RRM)-containing protein (TGME49_262620). This RRM-containing protein was also pulled
396 down with GCN5b acetyltransferase [55]. RRM-containing proteins are involved in post-transcriptional gene
397 expression processes, such as mRNA and rRNA processing, RNA export, translation, localization, stability, and
398 turnover [67]. In the case of acetylated peptide, it pulled down 2 specific proteins: a cyclin-dependent kinase
399 regulator (CDK_ TGME49_219832) and H3.3 histone variant (TGME49_218260). CDK is ortholog to a
400 *Neospora caninum* putative high mobility group protein (HMG_NCLIV_060770) and could be related to
401 transcription and cell cycle according to GO term analysis. CDKs have undergone an extraordinary degree of
402 evolutionary divergence and specialization and in yeast there is a number of different CDKs that
403 phosphorylate multiple substrates, thus regulating the cell-division cycle in response to different cellular cues
404 [68]. Also associated with the acetylated peptide H3.3 histone was found. H3.3 and H2A.Z are associated to
405 promoter regions flanking the nucleosome depleted region (NDR) of active genes [69]. Therefore, it may be
406 likely that acetylated H2A.Z and H2B.Z would associate to this variant histone in active promoters. However,
407 this association was not found in our genome wide analysis on tachyzoite stage [17]. Among the proteins
408 pulled down independent of the acetylation is the HAT GCN5A. GCN5A was shown to impact on H2A.Z
409 acetylation via crosstalk with H4 acetylation by means of bromodomain in p300 [70]. Future studies should

410 confirm the association of H2B.Z with GCN5A and stablish in this way a possible role of this histone in
411 regulation of gene expression.

412 In addition, CDKs have also been linked to mitosis [71, 72] and H3.3 is related to chromosome
413 segregation, nuclear structure, and the maintenance of genome integrity [73]. In this direction, it is
414 interesting that our pull-down assay has also retrieved, only for the acetylated peptide, other genes, all of
415 them associated to chromosome segregation (Table S1). Among them, peptidase c50 (TGME49_262825) a
416 separase or caspase-like protease. Separases are known to play a central role in the chromosome segregation
417 in yeast [74]. Structural maintenance of chromosomes (SMC) proteins -like RecF/RecN/SMC N terminal
418 domain-containing protein (TGME49_231170) found in our study- function together with other proteins in a
419 range of chromosomal transactions, including chromosome condensation, sister-chromatid cohesion,
420 recombination, DNA repair and epigenetic silencing of gene expression [75-77]. Finally, meiotic
421 recombination protein DMC1 family (TGME49_216400) was also retrieved in this pull down. This family of
422 proteins participate in meiotic recombination, specifically in homologous strand assimilation, which is
423 required for the resolution of meiotic double-strand breaks [78]. These findings are interesting, linking H2B.Z
424 and its N-tail acetylation to the mitotic and meiotic processes. Further studies are needed to shed light in
425 these subjects.

426 The decrease in acetyl-CoA in *T. gondii* leads to acetylation defects of several proteins including H2A.Z
427 and H2B.Z and could link histone PTM to nutritional stress [79]. An acetylation deficit could be a possible
428 physiological explanation for a positive charge patch in H2B.Z. Although the retrieval of acetyl-CoA
429 carboxylase ACC1 (TGME49_221320) by our peptides is tempting to speculate on the role of H2B.Z in sensing
430 this nutrient availability through lysine acetylation, the apicoplast localization makes it difficult to understand
431 this interaction. One possible explanation would be the presence of the histone in this organelle. The extra-
432 nuclear localization of histones was highly evidenced in other models [80-83]. Deficiencies in *Trypanosoma*
433 *cruzi* H2Bv histone variant amount present similar phenotypes as observed here, and some are also explained

434 in a putative extra-nuclear or extra-nucleosome function [84]. Interestingly, *T. gondii* H2B.Z peptides were
435 detected in extra-nuclear locations in ToxoDB: mitochondria, conoid and membrane fraction. To note, H2B.Z
436 abundance makes it the major H2B family histone [22], compared to H2A.Z variant.

437 It is relevant that these tachyzoites were able to generate a complete immune response, which only
438 happens when cells are invaded by tachyzoites and not with an infection with dead or lysed tachyzoites [85-
439 88]. In this sense, Toxovac® is a live attenuated vaccine used to prevent sheep congenital toxoplasmosis [89].
440 Recently, a Ca^{2+}-dependent protein kinase (CDPK) knock-out in Me49 type II strain was evaluated in mice as
441 a potential vaccine candidate [90]. The protection we observed in this work generated in mice facing an
442 infection with virulent RH tachyzoites is encouraging to continue with the proper assays needed for the
443 formulation of a vaccine.

444

445 # Conclusion

446 In this work, we have shown that N-terminal tail lysine acetylation of histone H2B.Z is important for
447 the normal progression of *Toxoplasma gondii* life cycle. The presence of 5 positive charges in the N-terminal
448 of H2B.Z is most likely to be detrimental for the parasite. This toxicity is not very high, allowing the parasite
449 to replicate, but conferring a lower fitness to the tachyzoite. Moreover, this lower fitness is traduced in a
450 higher sensitivity to DNA damage, a mis-regulation of gene expression conducing to a higher differentiation
451 rate *in vitro*, and also a complete lack of virulence when facing the immune response in mice. All these effects
452 are not explained by an heterochromatinization of DNA due to the interaction with the positive charges,
453 because we observed that nuclei are also smaller in c-Myc-A tachyzoites. Besides, the effects cannot be
454 explained by a dislocalization of the histone in the genome because the nucleosome is still constituted
455 normally. However, it is quite unlikely to find a physiologically a situation where the histone would be
456 completely unacetylated, and c-Myc-A tachyzoites may reflect the normal condition observed *in vivo*.

457 Therefore, the similarity observed between c-Myc-A and parental tachyzoites in most experiments
458 performed in this work, would confirm that in normal conditions H2B.Z is acetylated in *T. gondii*.

459 The findings in this work are not exclusively explained by regulation of gene expression. This is not
460 surprising, as it is known that histone proteins may exert other functions, related for example to cell division.
461 Even extra-nuclear functions are attributed to histones in many models, and research in this area could bring
462 new insights for *T. gondii* as well.

463 Having a better understanding of how chromatin and gene expression are modulated in *T. gondii* will
464 allow inferring about chromatin modulation in other parasites of the phylum as well as the possibility of
465 suggesting a novel mechanism of epigenetic regulation in organisms with complex life cycles that are
466 evolutionarily distant from fungi and vertebrates.

467

468

469

470 # Materials and methods

471 **Parasite culture and manipulation**

472 RHΔ*hxgprt* strain was used in all cases and grown in standard tachyzoite conditions *in vitro*: hTERT (ATCC®
473 CRL-4001, USA) monolayers were infected with tachyzoites and incubated with Dulbecco's modified Eagle
474 medium (DMEM, Invitrogen) supplemented with 1% fetal bovine serum (FBS, Internegocios S.A.,
475 Argentina) and penicillin (10,000 units/ml)-streptomycin (10 mg/ml) solution (Gibco, Argentina) at 37°C and
476 5% CO_2.

477 **Cloning over-expression strategy**

478 To generate the c-Myc-H2B.Z WT construct, the open reading frame (ORF) was amplified using the primers
479 F: 5'-ATGCATTCAGGGAAAGGTCCGGCACAG-3' and R: 5'-TTAATTAACTATGCACCAGAAGTCGTG-3'. For the
480 mutant constructs, reverse primer was the same, and forward was:
481 ATGCATTCAGGG**GCA**GGTCCGGCACAG**GCA**TCTCAGGCGGCG**GCGGCG**ACCGCCGGG**GCG**TCTCTGGGAC for c-
482 Myc-A, ATGCATTCAGGG**CGC**GGTCCGGCACAG**CGC**TCTCAGGCGGCG**CGCCGC**ACCGCCGGG**CGC**TCTCTGGGAC
483 for c-Myc-R, where lysine coding codons were replaced for alanine and arginine coding codons, respectively
484 (in bold type). NsiI and PacI restriction sites (underlined) were engineered into the 5' end of primers F and R,
485 respectively, to clone into *T. gondii* expression vector PTUB8mycGFPPfTailTy-HX (a kind gift of Dr. Dominique
486 Soldati, Université de Geneve) with a strong tubulin promoter. The resulting PCR product of the expected
487 size was removed using a Qiaex II Gel Extraction kit (Qiagen), cloned in pGEM-T vector (Promega) and
488 sequenced (Macrogen). The cloned ORF was digested with NsiI and PacI and ligated into the plasmid. The
489 final plasmids were electroporated into RH strain tachyzoites lacking hypoxanthine–xanthine guanine
490 phosphoribosyl transferase (RH∆*hxgprt*). Transgenic parasites were selected in mycophenolic acid (25 μg/ml,
491 Sigma) and xanthine (50 μg/ml, Sigma) and cloned by limiting dilution.

492 **CRISPR/Cas9 gene deletion strategy**

493 Single guide RNAs were designed directed to the N-terminal portion of the *h2bz* gene: F:
494 AAGTTGAGGCGGCGAAGAAGACCGCCG and R: AAAACGGCGGTCTTCTTCGCCGCCTCA. Bsa I restriction sites
495 were included (underlined). Both oligos were annealed and cloned into the pU6 CRISPR Universal plasmid
496 (kindly provided by Lourido´s Lab, Whitehead Institute), by using the Bsa I restriction site. The plasmids were
497 confirmed by PCR, using the gRNA as primers, were sequenced (Macrogen) and prepared for transfection in
498 *Toxoplasma*. In order to obtain a clean KO, oligos were also designed to amplify the DHFR selection cassette
499 from the pUPRT_DHFR plasmid available in the laboratory, with homology regions (20 bp underlined) to the
500 3´and 5´UTR of the *h2bz* gene (F:
501 GAAAGGTCCGGCACAGAAATCTCAGGCGGCGAAGAAGACCAAGCTTCGCCAGGCTGTAAATCC, and R:

502 GAATTCCCTCTCAACATCAAATTTCACCCCGTGGTTTATTCCTCATCCTGCAAGTGCATAGAAGGA). The PCR
503 amplification product was purified from agarose gel and used to co-transfect the parasites along with the
504 CRISPR plasmid. c-Myc-R and c-Myc-A tachyzoites (one clone for each one was selected) were transfected
505 and Pyrimethamine (1 μm, Sigma) was used for selection. Cas9 was detected in the nucleus of the parasites
506 after transfection by using α-Flag antibody (Sigma, F1804). Selection was continued until three passages and
507 cloning by limiting dilution was performed. Positive clones were selected by PCR with primers designed for
508 that purpose: TgH2Bv-upUTR-F: GTTGTCATGCGCATTTGCATCAC; TgH2Bv-downUTR-R:
509 GTGTGCACGCGTTATAATGAGCAC; Val-TgH2Bv-R: CATGCTCTTCTTCGACACACCAG; DHFRCX-F:
510 GTGGCATTTCACACAGTCTCACCTC; DHFRCX-R: AGACGCAGACGCATACAACGTTAG.

511 **Immunofluorescence assay (IFA)**

512 Intracellular tachyzoites grown in cover slips were fixed using cold methanol 100% for 8 min, washed with
513 PBS and blocked with 1% BSA. Primary antibody αrH2B.Z (rabbit), αrSag1 (mouse), αrHSP90 (rabbit), αrROP5
514 (rabbit), αrROP18 (rabbit) produced in the laboratory and αc-Myc (rabbit, abCam ab9106 or mouse, Santa
515 Cruz sc-42), αAcTubulin (mouse, Millipore MABT868) were incubated for 1 h at room temperature. After
516 several washes with PBS cover slips were incubated with secondary antibodies Alexa fluor goat anti-mouse
517 488 and anti-rabbit 594 (Invitrogen). DAPI was used to stain nuclei. Axio Imager.M2 Microscope Carl Zeiss
518 (Germany) with objective Plan-Apochromat 63x/1.40 Oil M27 and Video digital camera Zeiss 503
519 monochromatic 2.8 megapixeles, was used. Image J 1.53q (Fiji) software was used to process images.

520 **Western blot analysis**

521 Tachyzoites were collected, filtered, counted and lysed by 6 cycles of rapid freezing/defreeze in hypotonic
522 buffer, and boiled with LB for 5 minutes. 0.5 to 1×10^7 parasites were loaded per well and resolved by 15%
523 SDS-PAGE. Proteins were transferred to PVDF membrane for 1h at 100V. Western blot was then performed
524 as described [91]. The primary antibodies: αrH2B.Z [22], αrH2A.Z [23], αrROP5 (rabbit) and αrROP18 (rabbit)

525 were used at 1/5000, whereas α-c-Myc (rabbit, abCam ab9106) was used at 1/2000 and αrSag1 [88] 1/200
526 for 1 h at room temperature. αH3ac (rabbit, Millipore, 06-599B) 1/200, was incubated overnight. Appropriate
527 secondary antibodies were used: phosphatase alkaline-conjugated goat anti-mouse or anti-rabbit (Sigma)
528 along with the NBT and BCIP (Promega) detection system.

529 **Phenotypical assays**

530 For growth/competition assays, coverslips seeded with Htert cells were infected with a mix of 50% parental
531 (RHΔ*hxgprt*) and 50% of each clone. 3 coverslips per clone were infected with 0,05 to 0,1 tachyzoite per cell,
532 incubated 10 minutes on ice, and 2 hours at 37°C in incubator for invasion. Slides were washed twice with
533 PBS to remove tachyzoites that did not enter the cells, and fresh DMEM supplemented with 1% SFB was
534 added. Slides were fixed at different times, up to 96 hours and IFA was performed with α-c-Myc and α-Sag1
535 antibodies to distinguish between parental and c-Myc positive vacuoles. Number of c-Myc positive and total
536 vacuoles in at least 100 vacuoles, randomly choosing different fields of each slide were counted. In the case
537 of competition assays with genotoxic drugs treatment, the experiment was modified as follows: 3 slides per
538 clone mixture were fixed after 24 h, to stablish the initial percentage of c-Myc positive vacuoles. At this time
539 point, media was changed in the rest of the slides for DMEM supplemented with DMSO or drugs at the
540 concentrations indicated. These slides were fixed after 96 h, and IFA was performed and counted as explained
541 before.

542 For *in vitro* differentiation assays, in a similar way using Htert confluent slides, media was changed by DMEM
543 HEPES pH 8.1, after invasion with 1 parasite every 10 cells, accompanied with deprivation of CO_2. Media was
544 changed every day, and differentiation rate was estimated after 96 h by using *Dolichos Biflorus* Lectin
545 conjugated to Fluorescein (DLB 1:200, FL-1031; Vector Laboratories) to stain the wall of the cysts in formation
546 and α-Sag1 antibody to stain the tachyzoites. In the case of collection of parasites for RNA extraction,

547 differentiation assay was performed in a similar way, but in t25 dishes. After 48 or 96 h parasites were forced
548 out of the cells by 23G, 25G and 27G syringe passages.

549 For *in vivo* survival, virulence and differentiation assays, C57BL/6 female mice were used. For the use of
550 animals, C.I.C.U.A.E-UNSAM 10/22 was approved. Mice were maintained in optimal conditions in the
551 biotherium, with controlled temperature and free access to sterilized water and food. Infection was carried
552 out intra-peritoneal in 10 mice per group with 100, 1000 or 10000 tachyzoites of parental lines or clones,
553 depending on the assay. PBS was injected as negative control in five mice per experiment. Deceases were
554 registered along 30-35 days in each experiment, and signs of illness were monitored daily. Two mice from
555 each group (except PBS) were sacrificed at day 5 (when RH infected mice have symptoms of illness), and
556 intraperitoneal fluids were collected in order to detect acute *Toxoplasma* infection. Blood samples were
557 taken at days 0, 14, 21 and 35 and sera was frozen for ELISA assays. After sacrifice, surviving mice brains were
558 processed for cyst observance by optical microscopy. Also, a sample was stained using DLB and checked by
559 fluorescence microscopy.

560 In every phenotypical assay, three independent experiments were performed. One representative
561 experiment is shown.

562 **RT-PCR and RT-qPCR**

563 Tachyzoites or parasites exposed to 48 or 96 h differentiation stress as explained before were conserved in
564 TriZol (Invitrogen) solution at -80°C until use. All experiments were performed in three independent
565 replicates. RNA extraction was performed according to the manufacturer's instructions and cDNA was
566 obtained by means of MMLV reverse transcriptase (Promega) using oligo dT with the protocol provided with
567 the enzyme. For RT-PCR, primers used were: SAG1: Fw: TGAGAACCCGTGGCAGGGTAA; Rv:
568 GCTTTTTGACTCGGCTGGAA; TUB: Fw: ATGTTCCGTGGTCGCATGT; Rv: TGGGAATCCACTCAACGAAGT; ACTIN:
569 Fw: GGGCGGTTTCATGACCTAAA; Rv: ACGTATGATGCGCGAGAAAA; ROP5: Fw:

570 CTAGCTAGCATGGCGACGAAGCTCG; Rv: CCCAAGCTTTCAAGCGACTGAGGGCGCA; ROP18: Fw:
571 CTAGCTAGCATGTTTTCGGTACAGCGGCCA; Rv: GCCAAGCTTTTATTCTGTGTGGAGATGTTC.

572 For RT-qPCR primers used were: SAG1: Fw: TGAGAACCCGTGGCAGGGTAA; Rv: GCTTTTTGACTCGGCTGGAA;
573 BAG1: Fw:CAACGGAGCCATCGTTATCAAAGG; Rv: TAGAACGCCGTTGTCCATTG; LDH2:
574 Fw: ACAATGGCCCAGGCATTCT; Rv: CAATAAACATATCGTGAAGCCCATA; AP2IX-9:
575 Fw: GGGCGTTCTCAGCGTTCACT; Rv: GGCGCGTCTCATCTGTTTCA; AP2IV-3:
576 Fw: GAGCCCATTGACCCCATGAA; Rv: GGCTTCGCTTCTTTCCGTGA; BFD1: Fw:
577 ATGTCGGGAACGATGGTTTA; Rv: TCTTCACGGCATTCTCTGTG; TUB:
578 Fw: ATGTTCCGTGGTCGCATGT; Rv: TGGGAATCCACTCAACGAAGT; ACTIN: Fw: GGGCGGTTTCATGACCTAAA; Rv:
579 ACGTATGATGCGCGAGAAAA.

580 The primers were first assayed for efficiency using a pooled cDNA in 1 to 0.001 dilutions, and the threshold
581 was defined for each set of primers. Melt curves were also obtained for each set. For each set of experiments,
582 SybrGreen master solution (Roche) was used and qPCR was run in StepOne Real time equipment (Applied
583 Biosystems). Actin and tubulin were used as housekeeping genes and data was normalized to those genes
584 by Infostat software. For the experiments in figure 3, all sets of data were relativized to tachyzoite
585 amplification. For experiment shown in figure 7, data from the different clones was relativized to the
586 parental.

587 **ELISA assay**

588 Blood samples were extracted from surviving mice at days 0 (Pi), 14, 21 and 35. Sera was frozen until
589 processing for ELISA. TLA (Toxoplasma lysate antigen, obtained from fresh RH tachyzoites) in buffer
590 Carbonate (7,13g/L NaHCO3 + 1,59 g/L Na2CO3 pH 9,5) was used to immobilize 96 well plaques (Nunc
591 Immuno™ MicroWell™ 96 well solid plates, Sigma), o.n. at 4°C. After bocking with 5% non-fat milk in PBS-T
592 they were incubated with sera diluted 1:100 in the same solution. Total IgG (IgGt) and subtypes (IgG1, IgG2a

593 and IgG2b) HRP-conjugated anti-mouse, made in rat, were used 1:5000. Tetramethyl-bencidine (TMB,
594 Invitrogen) was used to reveal, and plaques were read after 20 min reaction at 655 nm in a Synergy H1. Data
595 was analyzed in GraphPad Prism v7. Sera from mice inoculated with PBS (negative control) or infected with
596 Me49 (positive control) were assayed.

597 **Co-Immunoprecipitation (Co-IP)**

598 Approximately 5×10^8 RHΔ*hxgprt* tachyzoites were used for each immunoprecipitation. Tachyzoites were
599 treated with micrococcal endonuclease (MNase) in order to obtain mononucleosomes as described [23] and
600 Co-IP was performed as described in Dalmasso et al [23] with minor modifications. Protease inhibitor cocktail
601 (Sigma) was added in every step. Mononucleosomes were incubated with Agarose c-Myc beads (abCam,
602 ab1253) overnight at 4°C. Immunocomplexes were washed twice with washing buffer 1 (50 mM Tris, pH8,
603 200 mM NaCl and 0.05 % Igepal100), twice with washing buffer 2 (50 mM Tris, pH8, 300 mM NaCl and 0.05
604 % Igepal100), and twice with buffer TE (10 mM Tris, pH8, 1 mM EDTA); then resuspended in 60 µl of SDS-
605 PAGE loading buffer. Samples were boiled for 5 min and 20 µl were loaded per well in a 15% SDS-PAGE gel
606 for immunoblotting. The absence of contaminating proteins was corroborated by Western blot with murine
607 anti-SAG1antibody [88]. Quantification of the bands was done with Image J 1.53q (Fiji) software.

608 **Tachyzoites nuclei size assay**

609 Three slides with confluent hTert cells were infected as explained before with parental or c-Myc-A/c-Myc-
610 R/c-Myc-WT-OE clones and let replicate for 24 hours. Slides were fixed and IFA was performed as explained
611 before using αrH2B.Z to stain nuclei. Images were processed with Image J 1.53q (Fiji) software to measure
612 the size of the nuclei, by delimiting them with the appropriate tool in at least 50 vacuoles in fields randomly
613 chosen, for each slide and each independent experiment. Data was graphed and statistical analyzed with
614 GraphPad Prism 8 software.

615 **Peptide synthesis and characterization**

616 Peptides were synthesized by solid-phase multiple peptide system using tea-bags with Fmoc/tBu strategy
617 according Guzmán [92], briefly: Rink amide resin (0.55 meq/g) was used as solid support and Fmoc amino acids,
618 including acetylated lysine (Iris Biotech). Peptides were couplet to biotin for their detection The peptide cleavage
619 was performed with a solution of Trifluoracetic acid/triisopropylsilane/1.2-ethandithiol /water (92.5 /2.5
620 /2.5/2.5), washed with cold ether dried and lyophilized. Peptides were characterized by HPLC and electrospray
621 ionization mass spectrometry, and purified by C18 cartridges (United Chemical Technologies, Bristol, PA, USA)
622 before use.
623 Peptides used in the pull-down assays were: Un-acetylated: GPAQKSQAAKKTAGKSLGPRK(Biotin)
624 Acetylated: GPAQKSQAAK(Ac)K(Ac)TAGKSLGPR-K(Biotin)
625 **Pull-down assays**

626 Pull-down experiments were performed as detailed in Wysocka [52] after nuclear extraction with NE-PER
627 commercial kit following manufacturer´s instructions (Thermo Scientific #78833) and run in SDS-PAGE for a
628 short time in order to avoid separation. Protein gels were fixed by soaking for 3 hr in 30% methanol, 2%
629 phosphoric acid. Then the gel was washed with deionized water 3 times, 5 minutes each. After removing the
630 deionized water, the staining solution (0.5 g/L Coomasie blue brilliant R250, 18% methanol, 17% $(NH_4)2SO_4$,
631 2% phosphoric acid) was added until covering the gel. It was stained for 1 h in gentle shaking. Then the gel
632 was rinsed in deionized water 3 times for 5 minutes each. The background staining was removed with 30%
633 methanol. The gel was stored in deionized water until use. Each lane of the gel was cut into individual slices.
634 Each band was then cut into 1 mm^3 cube and further treated with three washes of 50 mM NH_4HCO_3 in 50%
635 CH_3CN with 10 min incubations. Each group of gel cubes was then dehydrated in CH_3CN for 10 min and dried
636 in a Speed Vac. Protein samples were reduced by dithiothreitol (DTT) and alkylated by iodoacetamide [93]. A
637 solution of 10 ng/µL trypsin in 50 mM NH_4HCO_3 was used to re-swell the gel pieces completely at 4°C for 30
638 min, followed by a 37°C digestion overnight. A small amount of 10% formic acid was then added to stop the
639 digestion. The sample was then centrifuged at 2,800 x g, and the supernatant was collected for LC-MS/MS.

640 **LC-MS/MS Analysis**

641 A fused silica microcapillary LC column (15-cm long x 75-µm inside diameter) packed with Halo C18 reversed-
642 phase resin (2.7 µm particle size, 90 nm pore size, MichromBioresources.) was used with EASY-nLC 1200
643 system (Thermo Fisher). The nanospray ESI was fitted onto the Thermo Q-Exactive plus mass spectrometer
644 (Thermo Electron, San Jose, CA) that was operated in a Higher-energy C-trap dissociation mode to obtain
645 both MS and tandem MS (MS/MS) spectra. Two µL of tryptic peptide samples were loaded onto the
646 microcapillary column and separated by applying a gradient of 3-40% acetonitrile in 0.1% formic acid at a
647 flow rate of 300 nL/min for 80 min. Mass spectrometry data were acquired in a data-dependent top-10
648 acquisition mode, which uses a full MS scan from m/z 350-1700 at 70,000 resolution (automatic gain control
649 [AGC] target, 1e6; maximum ion time [max IT], 100 ms; profile mode). Resolution for dd-MS2 spectra was set
650 to 17,500 (AGC target: 1e5) with a maximum ion injection time of 50 ms. The normalized collision energy
651 was 27 eV.

652 **Protein Identification**

653 Obtained MS spectra were searched against the *T. gondii* ToxoDB-42 _TgondiiME49 protein database using
654 Proteome Discoverer 2.2 (Thermo Electron, San Jose, CA). The search parameters permitted a 10 ppm
655 peptide MS tolerance and a 0.02 Da MS/MS tolerance. Carboxymethylation of cysteines was set as a fixed
656 modification, and oxidation of methionine as a dynamic modification. Up to two missed tryptic peptide
657 cleavages were considered. The proteins for which the False Discovery Rate was less than 1% at the peptide
658 level were included in the following analysis. The raw data of all mass spectra had been submitted to the
659 MassIVE (https://massive.ucsd.edu/; Project accession: MassIVE MSV000091226).

660

661

662

663 **Author Contributions**: L.V. participated in all the experiments and analyses and wrote the first draft; D.M.
664 performed Crispr/Cas9 and some of the characterization experiments along with the pull-down experiments
665 with L.V. supervision; C.C. performed the DNA damage experiments and some of the transfections; A.G. was
666 involved in many of the experiments with technical support, and was in charge of RNA and cDNA preparation;
667 R.N. performed RT-PCR experiments and ELISAs with LV supervision; M.C.B. performed Co-IP experiments with
668 L.V. supervison; V.T. perfomed Rop5 and Rop18 antibodies and provided the respective primers for RT-PCR; F.G.
669 synthesized biotynilated peptides for pull down experiments; B.D. performed mass spectrometry analysis; K.K.
670 and W.J.S. participated in design of the study and manuscript final corrections; S.O.A. designed the study and
671 participated in its supervision. All authors have read and agreed to the published version of the manuscript.

672 **Funding**: This work was supported by the Ministerio Nacional de Ciencia y Tecnología (MINCyT): PICT 2015 1288
673 (S.O.A.), PICT 2018 2434 (L.V.), Consejo Nacional de Investigaciones Científicas y Tecnológicas (CONICET): PIP
674 11220150100145CO and 11220210100572CO (S.O.A., L.V.) and by National Institute of Health: NIH-NIAID
675 1R01AI129807 (S.O.A.) and AI152583 (to W.J.S.).

676 **Institutional Review Board Statement**: Not applicable.

677 **Informed Consent Statement**: Not applicable.

678 **Data Availability Statement**: The data that support the findings of this study are available from the
679 corresponding author upon reasonable request.

680 **Acknowledgments**: L. Vanagas (Researcher), D. Muñoz (Fellow), C. Cristaldi (Fellow), D. Ganuza (Technician), V.
681 Turowski (Researcher), and S.O. Angel (Researcher) are members of CONICET. S.O. Angel (Full) and L. Vanagas
682 (Adjunct) are Professors at Universidad Nacional General de San Martin (UNSAM). The Vermont Biomedical
683 Research Network (VBRN) Proteomics Facility is supported through NIH grant P20GM103449 from the INBRE
684 Program of the National Institute of General Medical Science (BD).

685 **Conflicts of interest**: The authors declare that there are no conflict of interest.

686

687 **FIGURES**

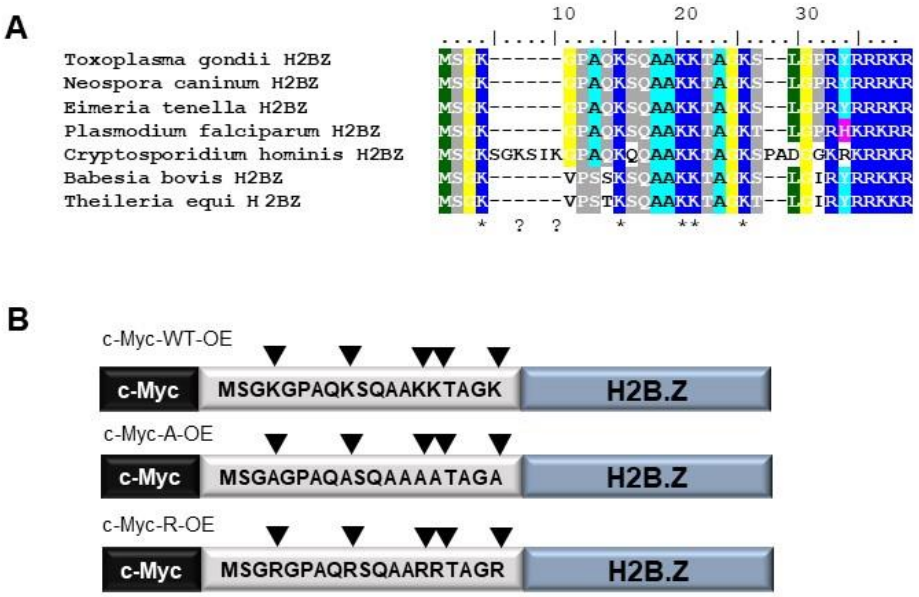

688

689 **Figure 1. H2B.Z N-tail acetylation and mutagenesis strategy. A.** Representative Apicomplexa H2B.Z N-tail
690 alignment. *Toxoplasma gondii* (TGME49_209910), *Neospora caninum* (NCLIV_004160), *Eimeria tenella*
691 (ETH_00030960), *Plasmodium falciparum* (PF3D7_0714000.1), *Cryptosporidium hominis* (cgd7_1700-RA),
692 *Babesia bovis* (BBOV_IV006840) and *Theileria equi* (BEWA_028110) H2B.Z protein sequences were aligned
693 by Clustal W. The N-tail region is shown. **B.** Scheme of the constructions generated in RHΔ*hxgprt* strain
694 tachyzoites. The N-terminal region is shown with the aminoacidic sequence, with or without mutations. All
695 constructions were performed associated to a tubulin promoter, in frame with a c-Myc tag in the N-
696 terminal.

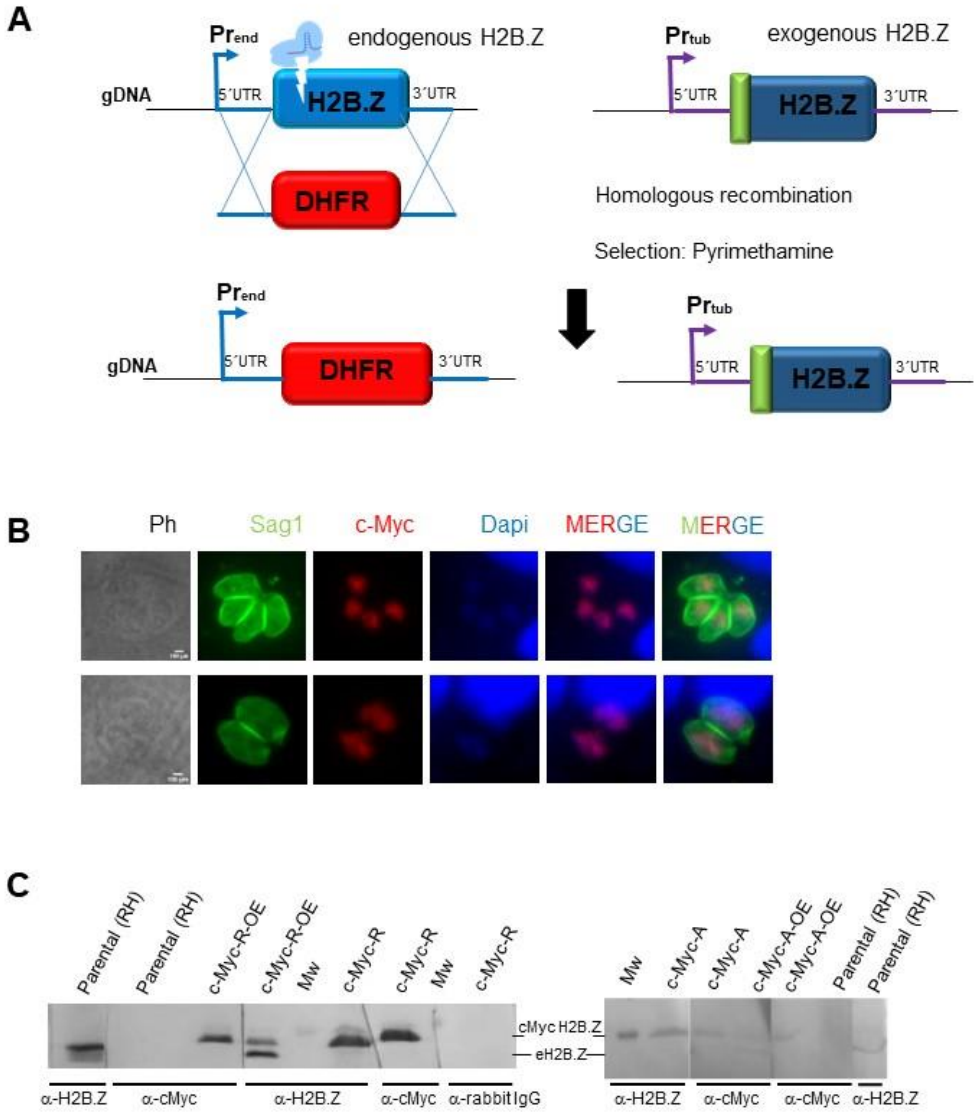

697

698 **Figure 2. H2B.Z gene deletion strategy**. **A.** CRISPR/Cas9 deletion of endogenous *h2b.z*, **s**trategy. Single guide
699 RNA was directed to the N-terminal region of H2B.Z. Tachyzoites of one clone c-Myc-R-OE and c-Myc-A-OE
700 were co-transfected with Crispr plasmid and a PCR product obtained with primers to amplify DHFR selection
701 cassette from pUPRT_DHFR plasmid with homology arms (20 pb) to 5´and 3´UTR of *h2b.z*. The scheme shows
702 the result of selection with Pyrimethamine and cloning, where parasites obtained replaced *h2b.z* by DHFR
703 cassette, and c-Myc-H2B.Z construction (with the corresponding mutations) remained. gDNA: genomic DNA;
704 Pr_{end}: endogenous promoter; Pr_{tub}: tubulin promoter. **B.** Immunofluorescence assay: coverslips seeded with

705 Htert cells at confluency were infected with 1 tachyzoite per cell of each obtained clone and fixed after 18-
706 24 hours. IFA was performed with α-cMyc (abCam), and α-Sag1 (mouse). α-IgG-mouse Alexa 488, and α-IgG
707 rabbit Alexa 564 were used 1:4000 for 30 minutes. DAPI was used to stain nuclei. Scale bar=5 μm. **C.** Western
708 blot assay. Clones confirmed by PCR were grown and lysed to run 0.5-1 x10^7 parasites per lane, transferred
709 to PVDF and assayed with indicated antibodies: α-c-Myc, α-H2B.Z, secondary α-rabbit IgG (negative control).
710 Over-expressing clones (c-Myc-R-OE and c-Myc-A-OE) used for transfection, as well as the parental (RH) were
711 loaded as controls. Mw: molecular weight marker (17 kDa band). eH2B.Z: endogenous H2B.Z.

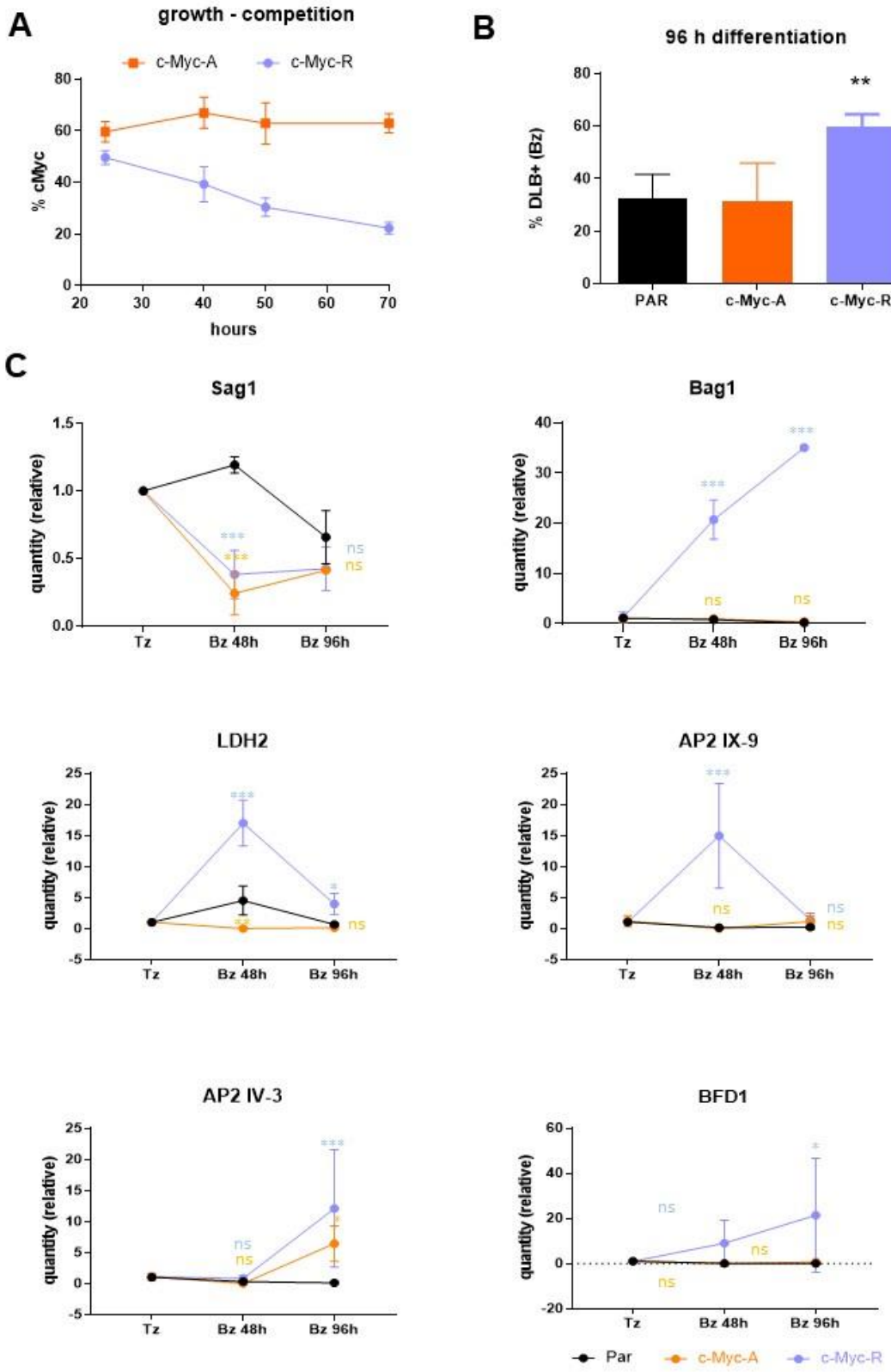
A
growth - competition
c-Myc-A
c-Myc-R
% cMyc
hours
B
96 h differentiation
% DLB+ (Bz)
PAR
c-Myc-A
c-Myc-R
C
Sag1
Bag1
LDH2
AP2 IX-9
AP2 IV-3
BFD1
quantity (relative)
Tz
Bz 48h
Bz 96h
Par
c-Myc-A
c-Myc-R

712

713 **Figure 3. *In vitro* growth and differentiation analysis on c-Myc-A and c-Myc-R**. **A.** Growth assay, performed
714 as explained in Materials and Methods. The percentage of c-Myc positive vacuoles is expressed as relative to
715 the total (α-Sag1), in at least 100 vacuoles per slide. Three slides per clone were counted. Representative
716 assay of three independent experiments. **B.** *In vitro* differentiation assay was performed as explained.
717 Percentage of DLB positive vacuoles was obtained after IFA with DLB and α-Sag1 to detect tachyzoites. PAR:
718 parental (RHΔ*hxgprt)*. Data was analyzed with Graphpad, and one-way Anova was performed. **: $p< 0.01$. **C.**
719 Tachyzoites (Tz) of parental (RHΔ*hxgprt*); c-Myc-A or c-Myc-R were freshly collected and conserved in Trizol
720 until processing. *In-vitro* differentiation was performed in dishes for 48 or 96 hours, and parasites were
721 collected and conserved in Trizol. RNA was extracted from each sample and cDNA was obtained by reverse
722 transcription with MMLV as explained in Materials and Methods. RT-qPCR was performed in Real time PCR
723 equipment (Applied Biosystems) with Sybr Green reagent with sets of primers indicated in each graph, using
724 tubulin and actin as housekeeping controls. Data was normalized to each of the housekeeping, and relative
725 quantities to tachyzoite in each sample is plotted for each of the genes studied. GraphPad Prism was used to
726 statisticaly analyze data, by two-way Anova. ***: $p< 0.0001$; **: $p< 0.01$; *: $p< 0.05$; ns: not significative.

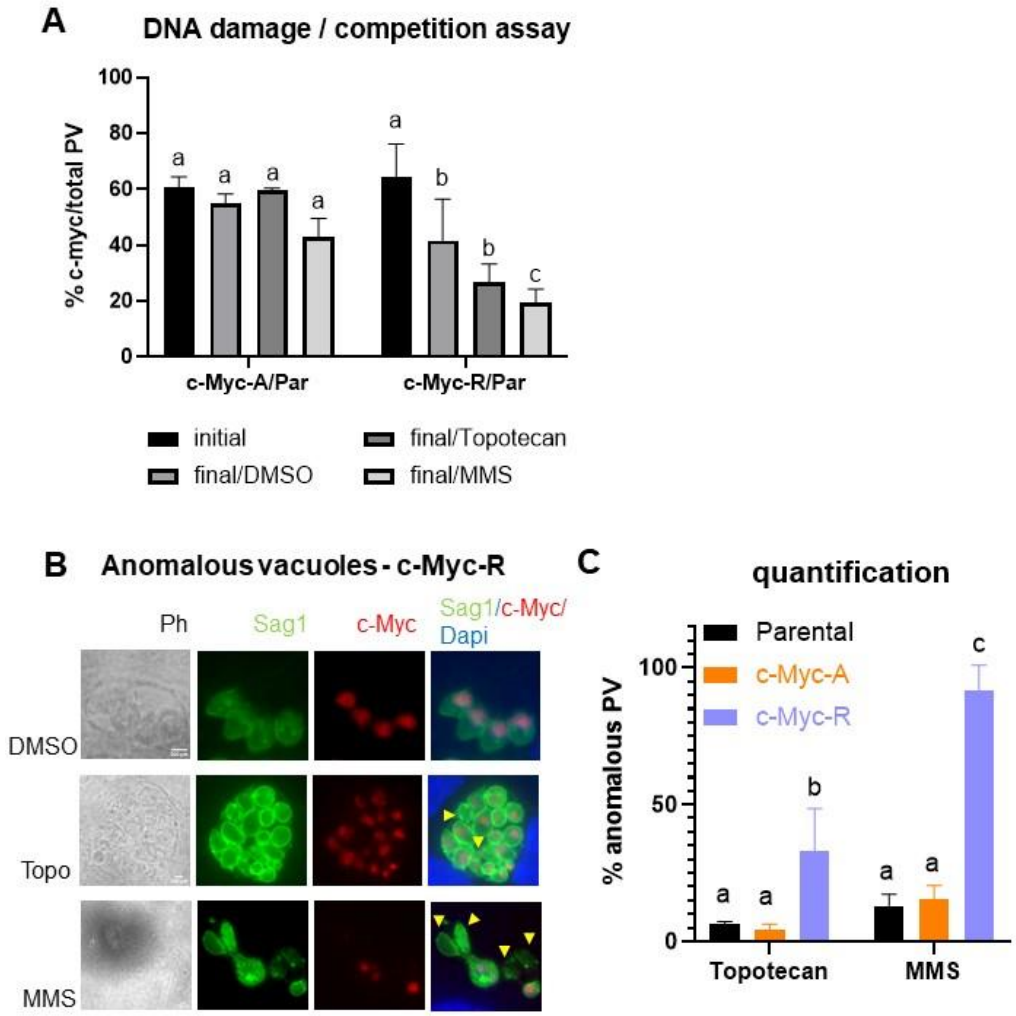

727

728 **Figure 4. H2B.Z acetylation status is important for DNA damage sensitivity. A.** Competition assay after DNA
729 damage induced by Topotecan (20 μM) or MMS (50 μM). Competition assay was performed as explained,
730 and IFA with anti-Sag1 for total vacuoles count and anti-cMyc for clones count was performed in three
731 independent experiments in triplicate. Graph shown corresponds to one representative assay. Initial: % of c-
732 Myc vacuoles of the total after 24 hours of infection with the mixture. Final: % of c-Myc vacuoles of the total
733 after 72 hours of treatment with each drug or DMSO as control. c-Myc-A/Par: mixture of c-Myc-A with
734 parental (RHΔ*hxgprt*) tachyzoites; c-Myc-R/Par: mixture of c-Myc-R with parental (RHΔ*hxgprt*) tachyzoites.
735 GraphPad Prism 8 statistical ANOVA analysis, multiple comparison where DMSO final is compared to initial
736 in each case and drugs data is compared to DMSO: a: ns; b: $p<0.05$; c: $p<0.01$. **B.** Vacuoles affected by drugs.

737 Representative images of most affected parasites (c-Myc-R) with both drug treatments. DMSO images are
738 included as control. Yellow arrowheads point to parasites with loss of genetic material. **C.** Quantification of
739 anomalous vacuoles. Anomalous and normal vacuoles were counted in at least 50 fields randomly chosen,
740 per clone, experiment and drug treatment. Results were plotted in GraphPad Prism 8 and statistical analysis
741 by Multiple comparisions was performed. a: ns; b: p<0.05; c: p<0.001.

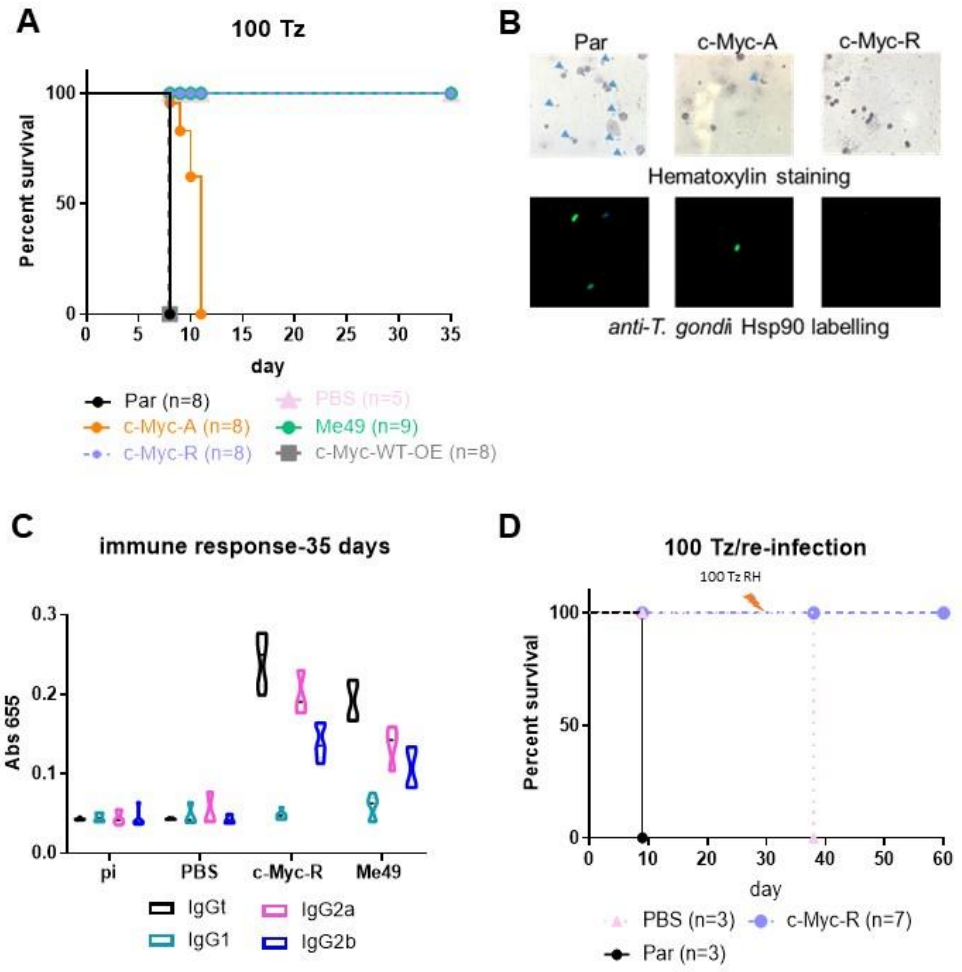

742

743 **Figure 5. c-Myc-R tachyzoites are not virulent i*n vivo* and elicit a protective immune response. A.** Survival
744 assay. 10 mice C57BL/6 were intra-peritoneal infected with either 100 tachyzoites of parental (RHΔ*hxgprt*),
745 and one clone of each KO line: c-Myc-R and c-Myc-A. As controls we also infected mice with c-Myc-WT-OE,
746 vehicle (PBS) and with Me49 tachyzoites (type II). The survival curve shown corresponds to one assay,

747 representative of three independent experiments. **B.** Acute infection. At day 5, 2 mice of each group were
748 sacrificed, and intra-peritoneal liquid was extracted and analyzed in the microscope, either by hematoxylin
749 staining (upper panel), or by IFA with α-HSP90 antibody (lower panel). Arrowheads in the upper panel show
750 tachyzoites. **C.** Evaluation of immune response by ELISA. Blood samples were extracted from surviving mice
751 at days 0 (Pi), 14, 21 and 35. Pooled sera from mice inoculated with PBS (negative control) or infected with
752 Me49 (positive control) were assayed. Total IgG and subtypes (IgG2a, IgG2b and IgG1) were analyzed. In the
753 graph only day 35 is shown. **D.** Re-infection assay. The indicated number of mice were infected with 1000
754 parental (Par) or c-Myc-R tachyzoites or inoculated with PBS. After 30 days, surviving mice were re-infected
755 with 100 parental RH tachyzoites. The survival curve shown corresponds to one assay, representative of three
756 independent experiments.

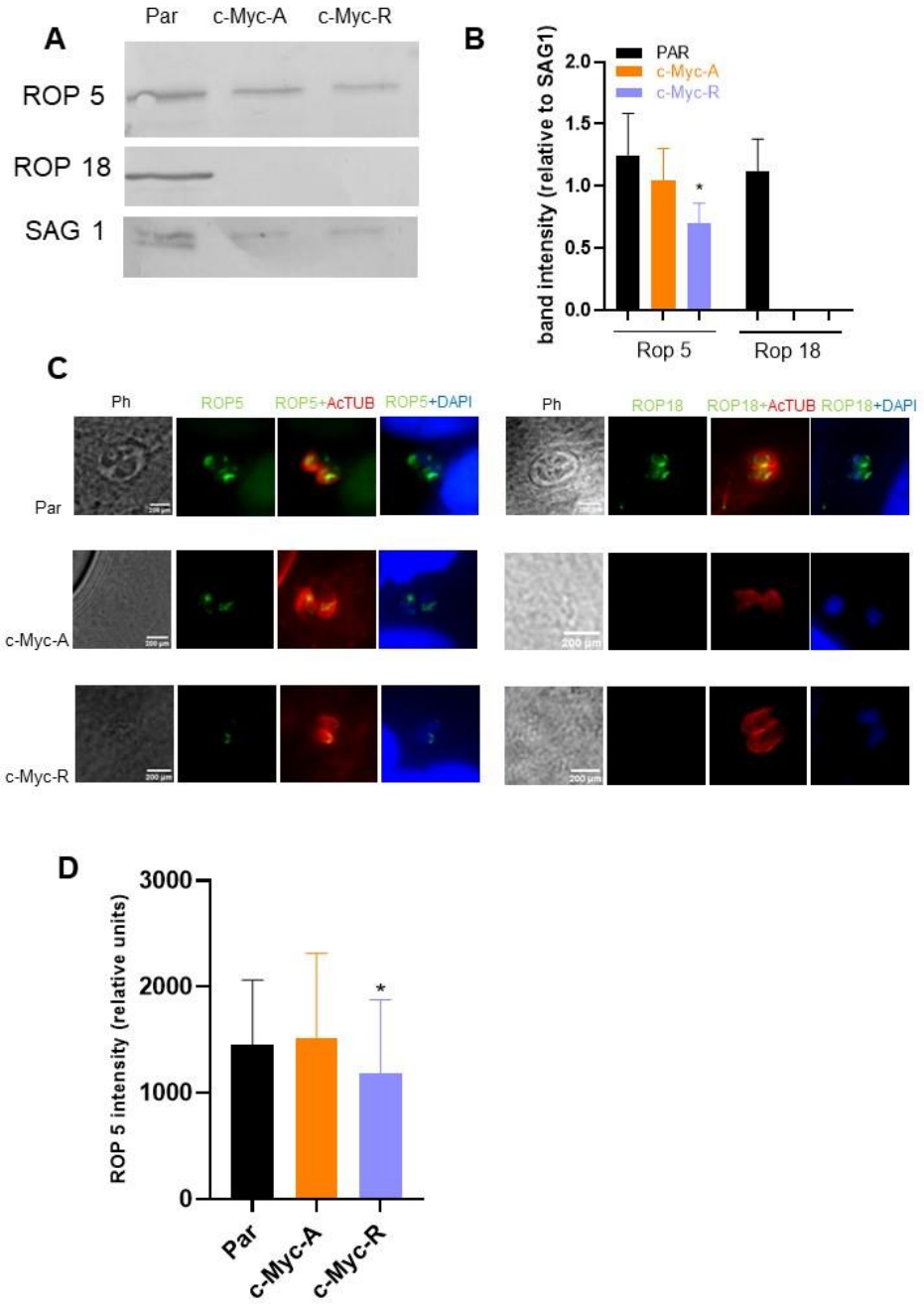

757

758 **Figure 6. Expression of ROP proteins is affected by H2B.Z acetylation. A.** Western blot identification of ROP5

759 and ROP18. The image is representative of three independent experiments, in which tachyzoite lysates of

760 parental (RHΔ*hxgprt*), c-Myc-A or c-Myc-R were run in SDS-PAGE, transferred to PVDF membrane and

761 assayed with anti Sag1 (charge control), anti Rop5 and anti-Rop18 antibodies. **B.** Quantification of band

762 intensities, relative to Sag1 band intensity in each lane. Image J software was employed to quantify relative
763 intensities and graphed with GraphPad Prism 8. Average plus SD of three independent assays is represented.
764 *: $p<0.05$. **C.** Immunofluorescence assay. Htert confluent slides were infected with tachyzoites of parental
765 (RHΔ*hxgprt*), c-Myc-A and c-Myc-R and fixed after 24 h for immunofluorescence analysis using anti Rop5 and
766 anti Rop18 antibodies (green). AcTubulin in red, was used to stain parasites and DAPI for the nuclei. **D.** Rop5
767 intensity quantification. Image J software was used to quantify the antibodies intensities in three
768 independent experiments, by triplicate, at least 10 vacuoles per slide. The graph shows the average intensity
769 in relative units; statistical analysis was performed by GraphPad Prism 8 software. *: $p<0.05$.

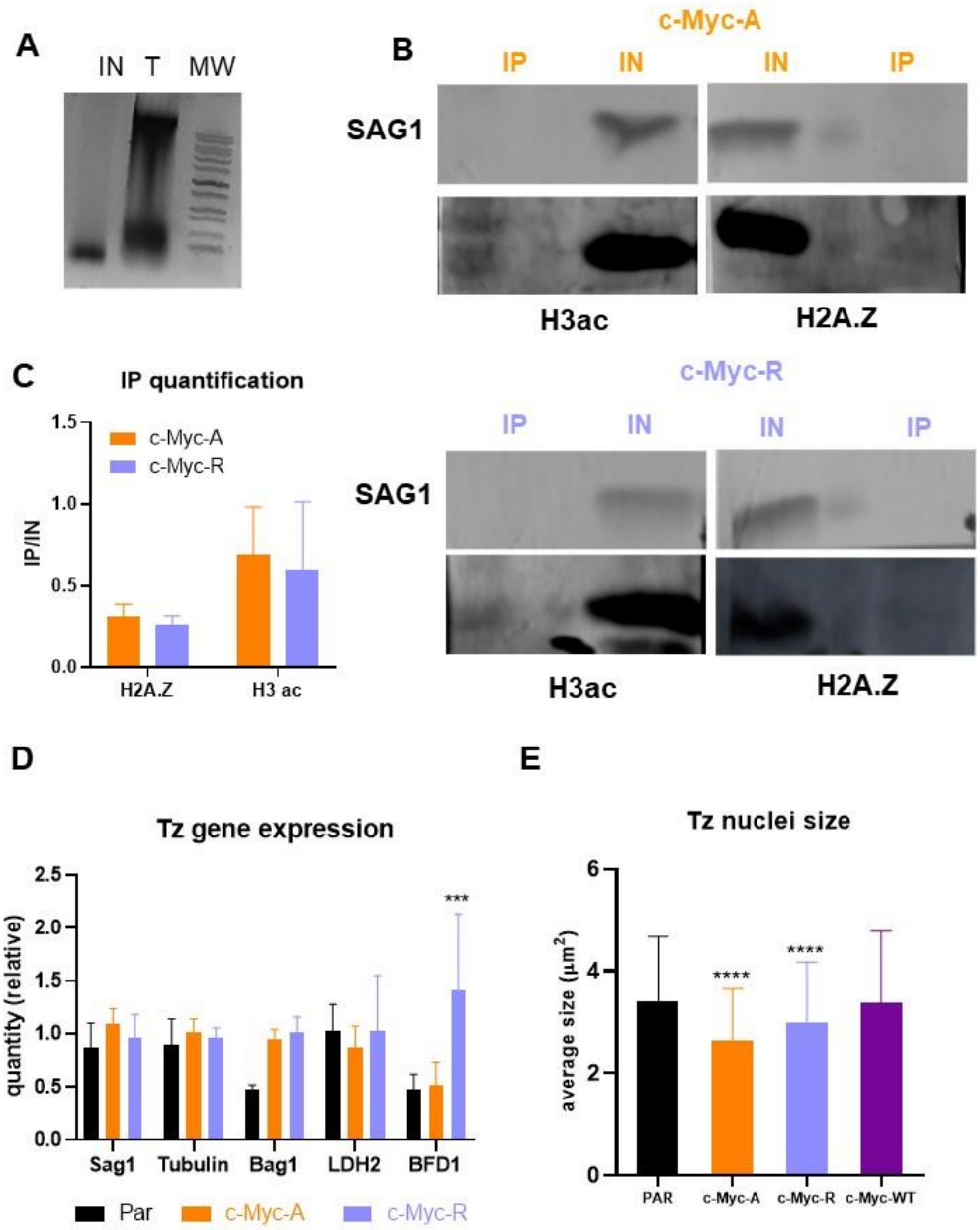

Figure 7. Nucleosome composition and chromatin structure is maintained in c-Myc-A and c-Myc-R. A. Mnase digestion of tachyzoites for co-immunoprecipitation analysis. Tachyzoites were MNase digested as explained in Materials and Methods, and an aliquot of the total tachyzoites and the digestion was precipitated and run in 1% agarose gel. A representative image of digestion is shown. **B.** Co-immunoprecipitation-WB analysis. Assays were performed in triplicate as explained in Materials and

776 Methods. A representative image of Western-blot analysis is shown for c-Myc-A and c-Myc-R. IP:
777 immunoprecipitation; IN: input. H3ac: western blot revealed with commercial anti H3acetylated antibody.
778 H2A.Z: western blot revealed with anti H2A.Z antibody performed in the lab. Sag1: western blot revealed
779 with anti Sag1 antibody. Color key: Orange for c-Myc-A; lilac for c-Myc-R. **C.** Quantification of western blot
780 band intensities. Image J software was used to quantificate intensities of H3ac and H2A.Z IP bands and
781 relativized to respective IN band intensities. Graph shows the relative intensities of three independent
782 experiments as the average plus SD for each antibody and clone, with the same key color as before. Graphpad
783 Prism 8 statistical analysis showed no significative differences between clones for both H3ac and H2A.Z
784 quantification. **D.** Tachyzoites gene expression. Tachyzoites (Tz) of parental (RHΔ*hxgprt*); c-Myc-A or c-Myc-
785 R were freshly collected in triplicate and conserved in Trizol until processing. RNA was extracted from each
786 sample and cDNA was obtained by reverse transcription with MMLV as explained in Materials and Methods.
787 RT-qPCR was performed in Real time PCR equipment (Applied Biosystems) with Sybr Green reagent with sets
788 of primers indicated in the graph, using actin as housekeeping control. Data was normalized to actin, and
789 relative quantities to RH tachyzoites in each sample is plotted for each of the genes studied. GraphPad Prism
790 was used to statisticaly analyze data, by two-way Anova. ***: $p< 0.0001$; ns: not significative. **E.** Tachyzoite
791 nuclei size. Tachyzoites of parental (RHΔ*hxgprt*), c-Myc-A, c-Myc-R or c-Myc-WT-OE were allowed to invade
792 hTert confluent slides and replicate for 20 h, and IFA was performed with α-H2B.Z antibody to detect the
793 nuclei. Image J software was used to measure the average nuclei size of at least 100 tachyzoites per slide, in
794 three independent experiments, and this was plotted and analyzed with Graphpad Prism 8, by two-way
795 ANOVA. ****: $p< 0.0001$.

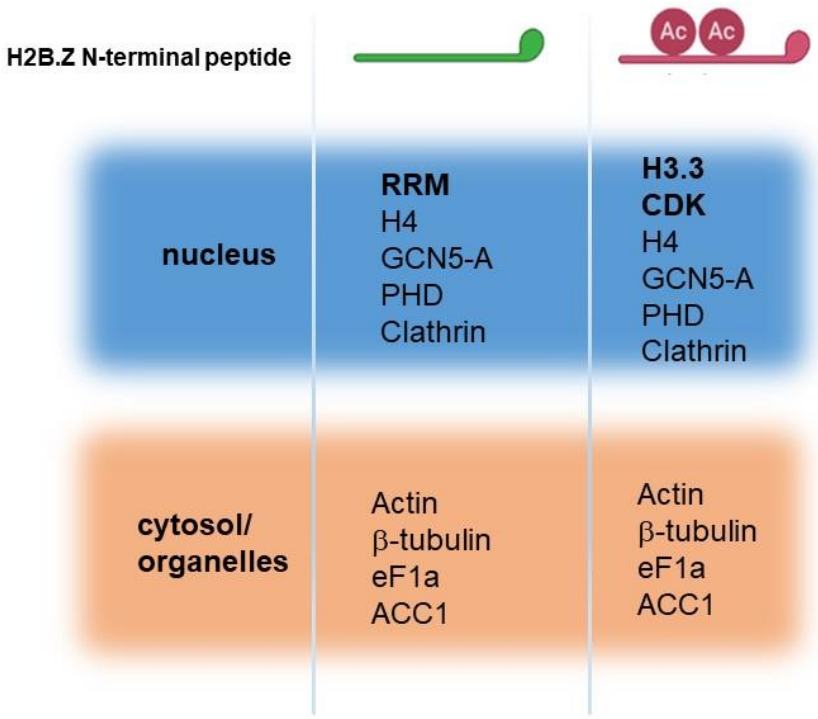

Figure 8. Identification of H2B.Z interacting proteins by pull-down assay. Scheme of the two different peptides synthesized is graphed above. Ac: acetylation. Most representative peptides retrieved in two independent assays for each peptide. Proteins are separated according to localization in nucleus or cytosol/organelles.

Supplementary figures

Figure S1

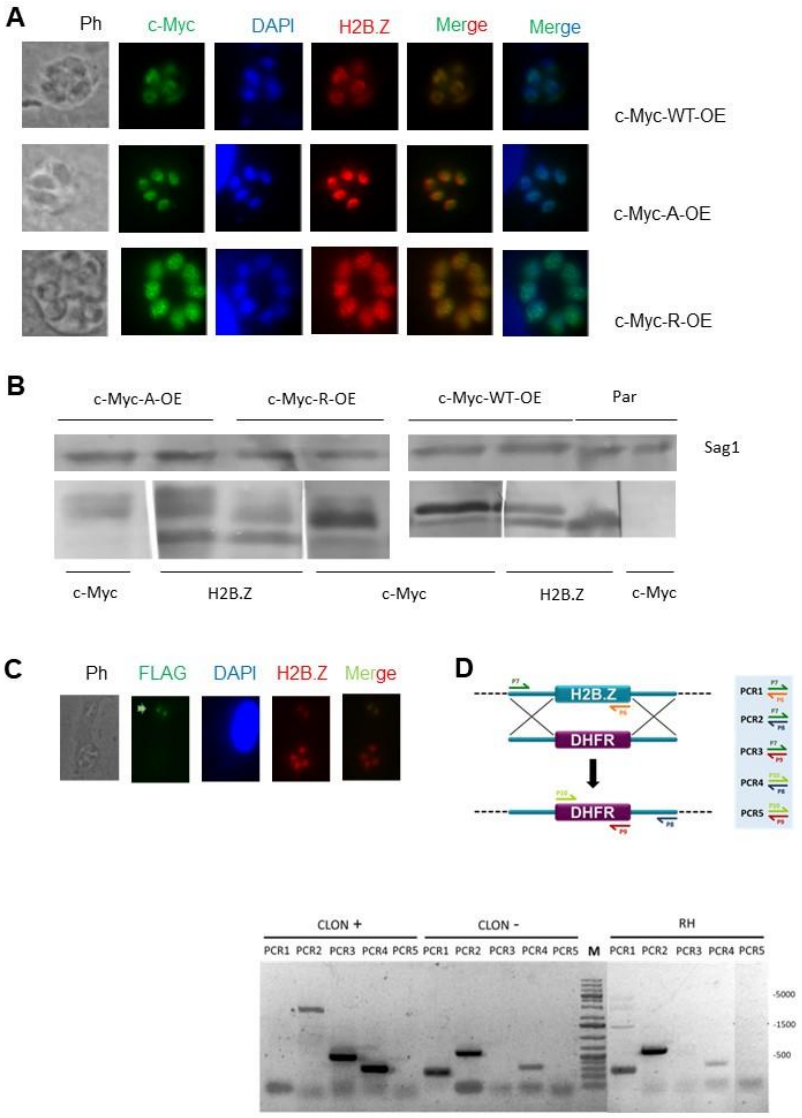

804

805 **Fig. S1. Controls for tachyzoite lines over-expressing H2B.Z WT or mutants and CRISPR/Cas9 deletion of**
806 **endogenous H2B.Z gene. A.** Immunofluorescence assay. Htert confluent slides were infected with the
807 different clones obtained and immunofluorescence was performed with anti c-Myc (green) and anti-H2B.Z
808 (red); DAPI was used to stain nuclei. Images show a representative IFA of one clone of each over-expressing
809 line obtained. **B.** Western-blot assay. One clone of each line and the parental were lysed and run in SDS-PAGE
810 for WB assay with anti-H2B.Z, anti-c-Myc and anti-Sag1 (charge control). **C.** Immunofluorescence after
811 transfection showing flag-CAS9 signal in the nucleus of one vacuole (green arrow). **B.** PCR selection of positive

812 clones. The scheme shows the primers designed for PCR detection of positive and negative clones. The image
813 corresponds to a representative PCR where a positive and a negative clone with the parental as control are
814 shown. PCR1-5: primers combinations for PCR shown in the scheme.

815

816 **Figure S2**

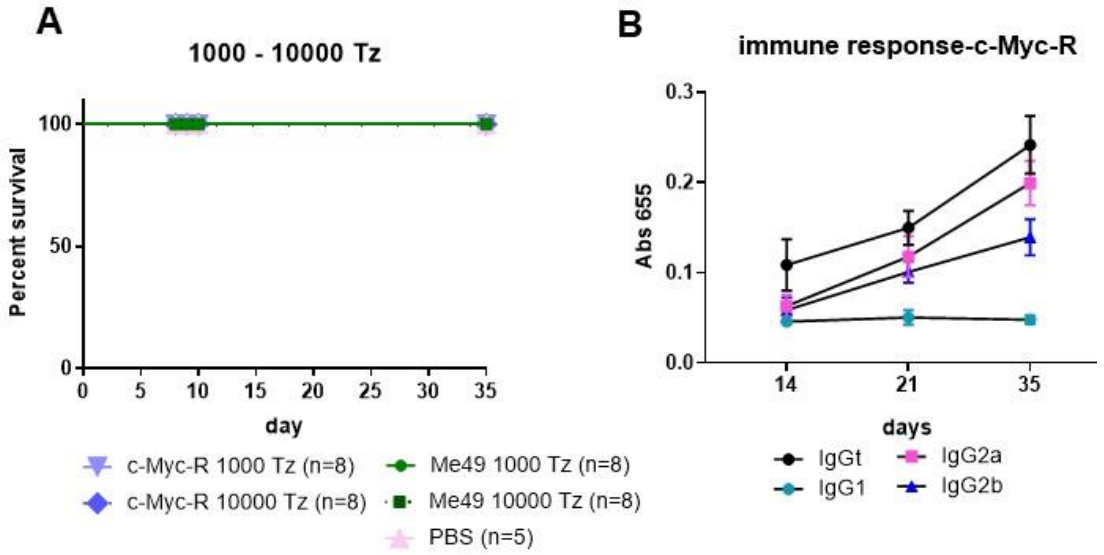

817

818 **Fig. S2. c-Myc-R tachyzoites up to 10,000 are unable to kill mice but immune response is triggered. A.**
819 Survival assay. 10 mice C57BL/6 were intra-peritoneal infected with either 1000 or 10000 tachyzoites of Me49
820 or c-Myc-R tachyzoites. Vehicle (PBS) was inoculated in 5 mice as control. The survival curve shown
821 corresponds to one assay, representative of three independent experiments. **B.** Evaluation of immune
822 response by ELISA. Assay shown in Fig. 5C, now showing data for 14, 21 and 35 days samples from mice
823 infeceted with c-Myc-R tachyzoites. Total IgG and subtypes (IgG2a, IgG2b and IgG1) were analyzed.

824 **Figure S3**

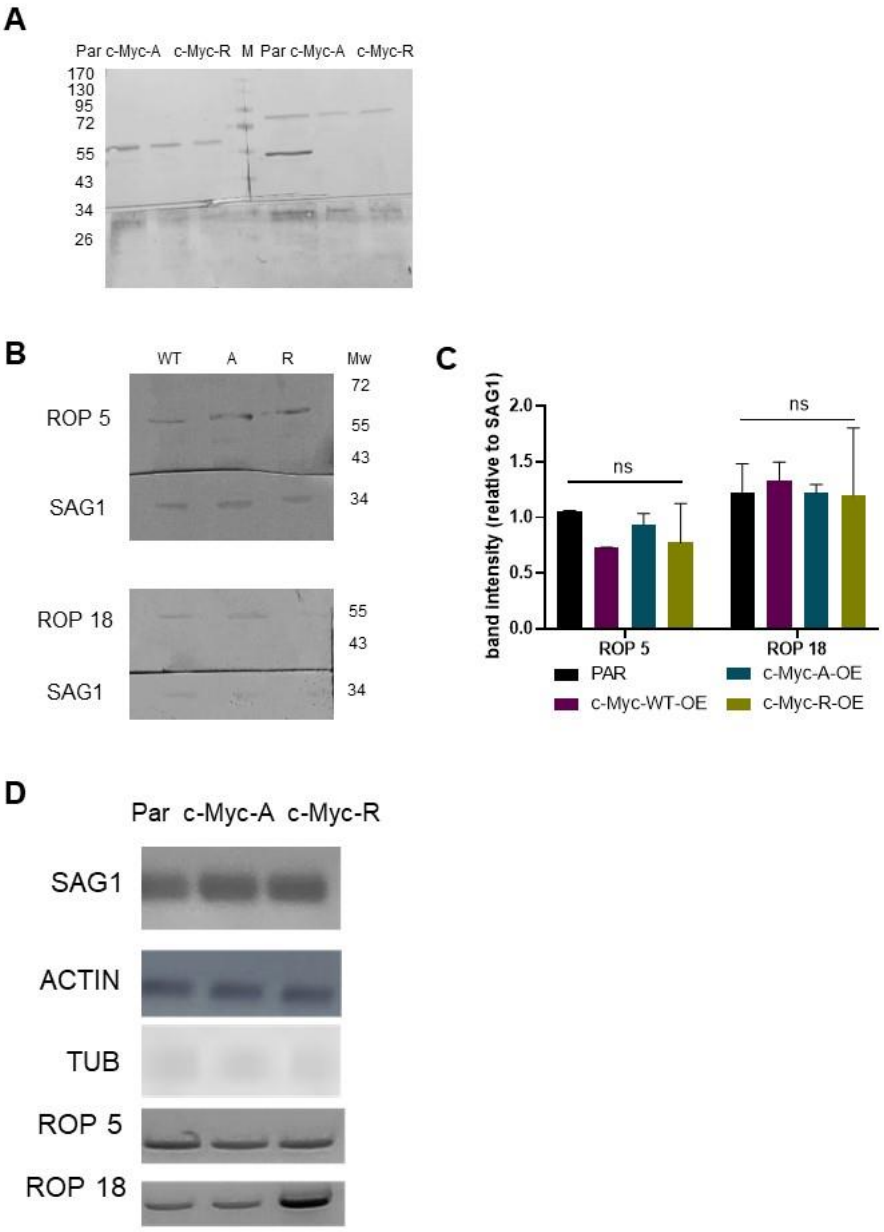

Fig. S3. Western blot analysis of ROP proteins. A. Complete image of Western blot shown in Fig. 5. **B.** Representative Western-blot of over-expressing lines. Antibodies against Rop5, Rop18 and Sag1 were used. WT: c-Myc-WT-OE; A: c-Myc-A-OE; R: c-Myc-R-OE. The upper bands detected with αRop18 are of higher molecular weight than Rop18 full length protein, being unspecific. However, the intensities are similar to Sag1, being a second charge control. **C.** Quantification of Rop5 and Rop18 bands, relativized to Sag1 band intensity in each lane, in two independent WB experiments with the OE lines, and statistical analysis by

832 GraphPad Prism 8. ns: not significative. **D.** RT-PCR. Tachyzoites of parental (RHΔ*hxgprt*), c-Myc-A and c-Myc-
833 R were collected by triplicate and conserved in TriZol until RNA extraction, and cDNA preparation. PCR was
834 run with primers for the genes indicated and ran in agarose gels. Image is representative of three
835 independent experiments.

836 **Figure S4**

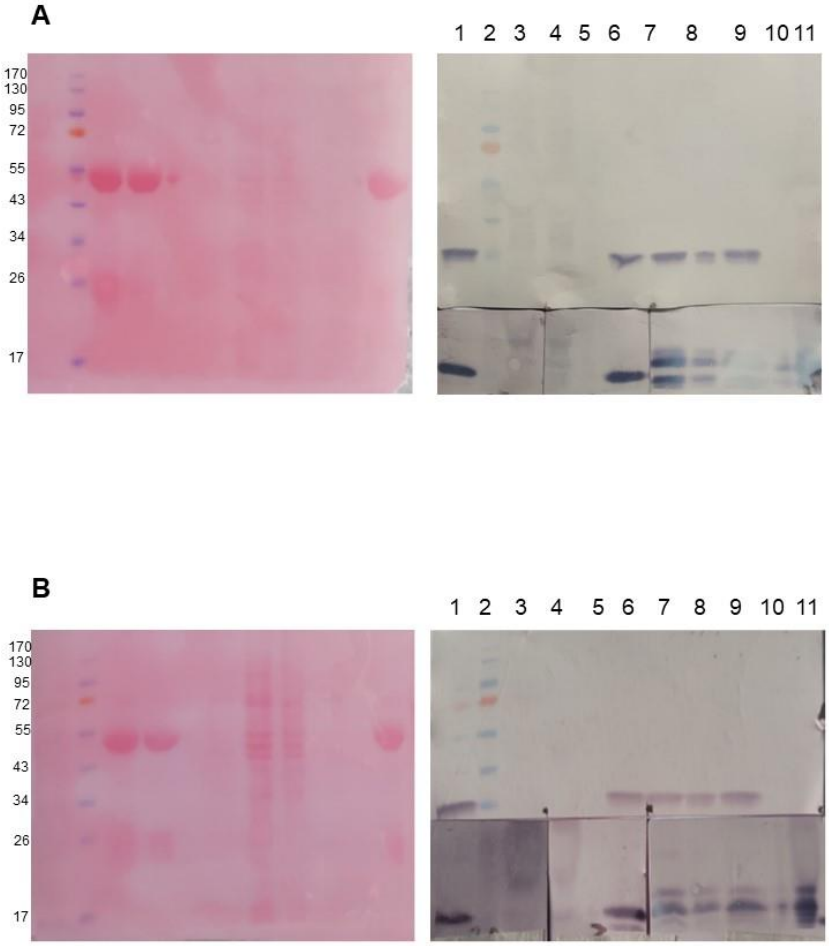

837

838 **Fig. S4. Co-immunoprecipitation assay. A.** Complete image of the Pounceau (left) and WB (right) shown in
839 Fig. 7 for c-Myc-A. **B.** Complete image of the Pounceau (left) and WB (right) shown in Fig. 7 for c-Myc-R. For
840 both images in lanes 1-11 was run: IN-M-IP-IP-space-IN-IN-T-NU-space-IP. IN: input; IP: immunoprecipitation;
841 T: total; NU: after immunoprecipitation, not bound to agarose beads. MW markers are indicated at the left.

842 # References

843 [1] Vanagas L, Jeffers V, Bogado SS, Dalmasso MC, Sullivan WJ, Jr., Angel SO. Toxoplasma histone
844 acetylation remodelers as novel drug targets. Expert review of anti-infective therapy. 2012;10:1189-
845 201.
846 [2] Mouveaux T, Rotili D, Boissavy T, Roger E, Pierrot C, Mai A, et al. A potent HDAC inhibitor blocks
847 Toxoplasma gondii tachyzoite growth and profoundly disrupts parasite gene expression. Int J
848 Antimicrob Agents. 2022;59:106526.
849 [3] Kim K. The Epigenome, Cell Cycle, and Development in Toxoplasma. Annual review of
850 microbiology. 2018;72:479-99.
851 [4] Pappas G, Roussos N, Falagas ME. Toxoplasmosis snapshots: global status of Toxoplasma gondii
852 seroprevalence and implications for pregnancy and congenital toxoplasmosis. Int J Parasitol.
853 2009;39:1385-94.
854 [5] Attias M, Teixeira DE, Benchimol M, Vommaro RC, Crepaldi PH, De Souza W. The life-cycle of
855 Toxoplasma gondii reviewed using animations. Parasit Vectors. 2020;13:588.
856 [6] Weiss LM, Kim K. The development and biology of bradyzoites of Toxoplasma gondii. Front Biosci.
857 2000;5:D391-405.
858 [7] Luft BJ, Remington JS. Toxoplasmic encephalitis in AIDS. Clin Infect Dis. 1992;15:211-22.
859 [8] Carlier Y, Truyens C, Deloron P, Peyron F. Congenital parasitic infections: a review. Acta Trop.
860 2012;121:55-70.
861 [9] Brynska A, Tomaszewicz-Libudzic E, Wolanczyk T. Obsessive-compulsive disorder and acquired
862 toxoplasmosis in two children. Eur Child Adolesc Psychiatry. 2001;10:200-4.
863 [10] Miman O, Mutlu EA, Ozcan O, Atambay M, Karlidag R, Unal S. Is there any role of Toxoplasma
864 gondii in the etiology of obsessive-compulsive disorder? Psychiatry Res. 2010;177:263-5.
865 [11] Yolken RH, Dickerson FB, Fuller Torrey E. Toxoplasma and schizophrenia. Parasite Immunol.
866 2009;31:706-15.
867 [12] Vittecoq M, Elguero E, Lafferty KD, Roche B, Brodeur J, Gauthier-Clerc M, et al. Brain cancer
868 mortality rates increase with Toxoplasma gondii seroprevalence in France. Infect Genet Evol.
869 2012;12:496-8.
870 [13] de Haan L, Sutterland AL, Schotborgh JV, Schirmbeck F, de Haan L. Association of Toxoplasma
871 gondii Seropositivity With Cognitive Function in Healthy People: A Systematic Review and Meta-
872 analysis. JAMA Psychiatry. 2021;78:1103-12.
873 [14] Waldman BS, Schwarz D, Wadsworth MH, 2nd, Saeij JP, Shalek AK, Lourido S. Identification of
874 a Master Regulator of Differentiation in Toxoplasma. Cell. 2020;180:359-72 e16.
875 [15] Jeffers V, Tampaki Z, Kim K, Sullivan WJ, Jr. A latent ability to persist: differentiation in
876 Toxoplasma gondii. Cellular and molecular life sciences : CMLS. 2018;75:2355-73.
877 [16] Bougdour A, Maubon D, Baldacci P, Ortet P, Bastien O, Bouillon A, et al. Drug inhibition of
878 HDAC3 and epigenetic control of differentiation in Apicomplexa parasites. The Journal of
879 experimental medicine. 2009;206:953-66.
880 [17] Nardelli SC, Silmon de Monerri NC, Vanagas L, Wang X, Tampaki Z, Sullivan WJ, Jr., et al.
881 Genome-wide localization of histone variants in Toxoplasma gondii implicates variant exchange in
882 stage-specific gene expression. BMC genomics. 2022;23:128.
883 [18] Santisteban MS, Kalashnikova T, Smith MM. Histone H2A.Z regulats transcription and is partially
884 redundant with nucleosome remodeling complexes. Cell. 2000;103:411-22.
885 [19] Oberdoerffer P, Miller KM. Histone H2A variants: Diversifying chromatin to ensure genome
886 integrity. Semin Cell Dev Biol. 2022.

887 [20] Xu Y, Ayrapetov MK, Xu C, Gursoy-Yuzugullu O, Hu Y, Price BD. Histone H2A.Z controls a critical
888 chromatin remodeling step required for DNA double-strand break repair. Mol Cell. 2012;48:723-33.
889 [21] Fenoy IM, Bogado SS, Contreras SM, Gottifredi V, Angel SO. The Knowns Unknowns: Exploring
890 the Homologous Recombination Repair Pathway in Toxoplasma gondii. Front Microbiol. 2016;7:627.
891 [22] Dalmasso MC, Echeverria PC, Zappia MP, Hellman U, Dubremetz JF, Angel SO. Toxoplasma
892 gondii has two lineages of histones 2b (H2B) with different expression profiles. Molecular and
893 biochemical parasitology. 2006;148:103-7.
894 [23] Dalmasso MC, Onyango DO, Naguleswaran A, Sullivan WJ, Jr., Angel SO. Toxoplasma H2A
895 variants reveal novel insights into nucleosome composition and functions for this histone family. J
896 Mol Biol. 2009;392:33-47.
897 [24] Dalmasso MC, Sullivan WJ, Jr., Angel SO. Canonical and variant histones of protozoan parasites.
898 Frontiers in bioscience. 2011;16:2086-105.
899 [25] Petter M, Selvarajah SA, Lee CC, Chin WH, Gupta AP, Bozdech Z, et al. H2A.Z and H2B.Z double-
900 variant nucleosomes define intergenic regions and dynamically occupy var gene promoters in the
901 malaria parasite Plasmodium falciparum. Molecular microbiology. 2013;87:1167-82.
902 [26] Lowell JE, Kaiser F, Janzen CJ, Cross GA. Histone H2AZ dimerizes with a novel variant H2B and is
903 enriched at repetitive DNA in Trypanosoma brucei. J Cell Sci. 2005;118:5721-30.
904 [27] Sidik SM, Huet D, Ganesan SM, Huynh MH, Wang T, Nasamu AS, et al. A Genome-wide CRISPR
905 Screen in Toxoplasma Identifies Essential Apicomplexan Genes. Cell. 2016;166:1423-35 e12.
906 [28] Nardelli SC, Che FY, Silmon de Monerri NC, Xiao H, Nieves E, Madrid-Aliste C, et al. The histone
907 code of Toxoplasma gondii comprises conserved and unique posttranslational modifications. mBio.
908 2013;4:e00922-13.
909 [29] Giaimo BD, Ferrante F, Herchenrother A, Hake SB, Borggrefe T. The histone variant H2A.Z in
910 gene regulation. Epigenetics & chromatin. 2019;12:37.
911 [30] Talbert PB, Henikoff S. Histone variants--ancient wrap artists of the epigenome. Nature reviews
912 Molecular cell biology. 2010;11:264-75.
913 [31] Bruce K, Myers FA, Mantouvalou E, Lefevre P, Greaves I, Bonifer C, et al. The replacement
914 histone H2A.Z in a hyperacetylated form is a feature of active genes in the chicken. Nucleic Acids
915 Res. 2005;33:5633-9.
916 [32] Binda O, Sevilla A, LeRoy G, Lemischka IR, Garcia BA, Richard S. SETD6 monomethylates H2AZ
917 on lysine 7 and is required for the maintenance of embryonic stem cell self-renewal. Epigenetics.
918 2013;8:177-83.
919 [33] Law C, Cheung P. Expression of Non-acetylatable H2A.Z in Myoblast Cells Blocks Myoblast
920 Differentiation through Disruption of MyoD Expression. J Biol Chem. 2015;290:13234-49.
921 [34] Valdes-Mora F, Song JZ, Statham AL, Strbenac D, Robinson MD, Nair SS, et al. Acetylation of
922 H2A.Z is a key epigenetic modification associated with gene deregulation and epigenetic remodeling
923 in cancer. Genome research. 2012;22:307-21.
924 [35] Whittle CM, McClinic KN, Ercan S, Zhang X, Green RD, Kelly WG, et al. The genomic distribution
925 and function of histone variant HTZ-1 during C. elegans embryogenesis. PLoS Genet.
926 2008;4:e1000187.
927 [36] Updike DL, Mango SE. Temporal regulation of foregut development by HTZ-1/H2A.Z and PHA-
928 4/FoxA. PLoS Genet. 2006;2:e161.
929 [37] Ridgway P, Brown KD, Rangasamy D, Svensson U, Tremethick DJ. Unique residues on the H2A.Z
930 containing nucleosome surface are important for Xenopus laevis development. J Biol Chem.
931 2004;279:43815-20.
932 [38] Myers FA, Chong W, Evans DR, Thorne AW, Crane-Robinson C. Acetylation of histone H2B
933 mirrors that of H4 and H3 at the chicken beta-globin locus but not at housekeeping genes. J Biol
934 Chem. 2003;278:36315-22.

935 [39] Miao J, Fan Q, Cui L, Li J, Li J, Cui L. The malaria parasite Plasmodium falciparum histones:
936 organization, expression, and acetylation. Gene. 2006;369:53-65.
937 [40] Trelle MB, Salcedo-Amaya AM, Cohen AM, Stunnenberg HG, Jensen ON. Global histone analysis
938 by mass spectrometry reveals a high content of acetylated lysine residues in the malaria parasite
939 Plasmodium falciparum. Journal of proteome research. 2009;8:3439-50.
940 [41] Radke JB, Lucas O, De Silva EK, Ma Y, Sullivan WJ, Jr., Weiss LM, et al. ApiAP2 transcription factor
941 restricts development of the Toxoplasma tissue cyst. Proc Natl Acad Sci U S A. 2013;110:6871-6.
942 [42] Hong DP, Radke JB, White MW. Opposing Transcriptional Mechanisms Regulate Toxoplasma
943 Development. mSphere. 2017;2.
944 [43] Gursoy-Yuzugullu O, Ayrapetov MK, Price BD. Histone chaperone Anp32e removes H2A.Z from
945 DNA double-strand breaks and promotes nucleosome reorganization and DNA repair. Proc Natl
946 Acad Sci U S A. 2015;112:7507-12.
947 [44] Morillo-Huesca M, Clemente-Ruiz M, Andujar E, Prado F. The SWR1 histone replacement
948 complex causes genetic instability and genome-wide transcription misregulation in the absence of
949 H2A.Z. PloS one. 2010;5:e12143.
950 [45] Munera Lopez J, Ganuza A, Bogado SS, Munoz D, Ruiz DM, Sullivan WJ, Jr., et al. Evaluation of
951 ATM Kinase Inhibitor KU-55933 as Potential Anti-Toxoplasma gondii Agent. Frontiers in cellular and
952 infection microbiology. 2019;9:26.
953 [46] Angel SO, Vanagas L, Ruiz DM, Cristaldi C, Saldarriaga Cartagena AM, Sullivan WJJ. Emerging
954 Therapeutic Targets Against Toxoplasma gondii: Update on DNA Repair Response Inhibitors and
955 Genotoxic Drugs. Front Cell Infect Microbiol. 2020;10.
956 [47] Behnke MS, Fentress SJ, Mashayekhi M, Li LX, Taylor GA, Sibley LD. The polymorphic
957 pseudokinase ROP5 controls virulence in Toxoplasma gondii by regulating the active kinase ROP18.
958 PLoS pathogens. 2012;8:e1002992.
959 [48] Etheridge RD, Alaganan A, Tang K, Lou HJ, Turk BE, Sibley LD. The Toxoplasma pseudokinase
960 ROP5 forms complexes with ROP18 and ROP17 kinases that synergize to control acute virulence in
961 mice. Cell host & microbe. 2014;15:537-50.
962 [49] Reese ML, Zeiner GM, Saeij JP, Boothroyd JC, Boyle JP. Polymorphic family of injected
963 pseudokinases is paramount in Toxoplasma virulence. Proc Natl Acad Sci U S A. 2011;108:9625-30.
964 [50] Saeij JP, Boyle JP, Coller S, Taylor S, Sibley LD, Brooke-Powell ET, et al. Polymorphic secreted
965 kinases are key virulence factors in toxoplasmosis. Science. 2006;314:1780-3.
966 [51] Fentress SJ, Behnke MS, Dunay IR, Mashayekhi M, Rommereim LM, Fox BA, et al.
967 Phosphorylation of immunity-related GTPases by a Toxoplasma gondii-secreted kinase promotes
968 macrophage survival and virulence. Cell host & microbe. 2010;8:484-95.
969 [52] Wysocka J. Identifying novel proteins recognizing histone modifications using peptide pull-
970 down assay. Methods. 2006;40:339-43.
971 [53] Croken MM, Nardelli SC, Kim K. Chromatin modifications, epigenetics, and how protozoan
972 parasites regulate their lives. Trends Parasitol. 2012;28:202-13.
973 [54] Croken MM, Qiu W, White MW, Kim K. Gene Set Enrichment Analysis (GSEA) of Toxoplasma
974 gondii expression datasets links cell cycle progression and the bradyzoite developmental program.
975 BMC genomics. 2014;15:515.
976 [55] Wang J, Dixon SE, Ting LM, Liu TK, Jeffers V, Croken MM, et al. Lysine acetyltransferase GCN5b
977 interacts with AP2 factors and is required for Toxoplasma gondii proliferation. PLoS pathogens.
978 2014;10:e1003830.
979 [56] Jeffers V, Gao H, Checkley LA, Liu Y, Ferdig MT, Sullivan WJ, Jr. Garcinol Inhibits GCN5-Mediated
980 Lysine Acetyltransferase Activity and Prevents Replication of the Parasite Toxoplasma gondii.
981 Antimicrobial agents and chemotherapy. 2016;60:2164-70.

982 [57] Huang S, Holmes MJ, Radke JB, Hong DP, Liu TK, White MW, et al. Toxoplasma gondii AP2IX-4
983 Regulates Gene Expression during Bradyzoite Development. mSphere. 2017;2.
984 [58] Khelifa AS, Guillen Sanchez C, Lesage KM, Huot L, Mouveaux T, Pericard P, et al. TgAP2IX-5 is a
985 key transcriptional regulator of the asexual cell cycle division in Toxoplasma gondii. Nature
986 communications. 2021;12:116.
987 [59] Sindikubwabo F, Ding S, Hussain T, Ortet P, Barakat M, Baumgarten S, et al. Modifications at
988 K31 on the lateral surface of histone H4 contribute to genome structure and expression in
989 apicomplexan parasites. eLife. 2017;6.
990 [60] Gissot M, Kelly KA, Ajioka JW, Greally JM, Kim K. Epigenomic modifications predict active
991 promoters and gene structure in Toxoplasma gondii. PLoS pathogens. 2007;3:e77.
992 [61] Ren Q, Gorovsky MA. Histone H2A.Z acetylation modulates an essential charge patch. Mol Cell.
993 2001;7:1329-35.
994 [62] Ren Q, Gorovsky MA. The nonessential H2A N-terminal tail can function as an essential charge
995 patch on the H2A.Z variant N-terminal tail. Mol Cell Biol. 2003;23:2778-89.
996 [63] Macadangdang BR, Oberai A, Spektor T, Campos OA, Sheng F, Carey MF, et al. Evolution of
997 histone 2A for chromatin compaction in eukaryotes. eLife. 2014;3.
998 [64] Severo V, Souza R, Vitorino F, Cunha J, Avila A, Arrizabalaga G, et al. Previously Unidentified
999 Histone H1-Like Protein Is Involved in Cell Division and Ribosome Biosynthesis in Toxoplasma gondii.
1000 mSphere. 2022;7:e0040322.
1001 [65] Sarah Sokol Borrelli SMR, Katherine G. Sharp, Leah F. Cabo, Hisham S. Alrubaye, Bruno
1002 Martorelli Di Genova and Jon P. Boyle. A transcriptional network required for Toxoplasma gondii
1003 tissue cyst formation is dispensable for long-term persistence. bioRxiv. 2022.
1004 [66] M. Haley Licon CJG, Sundeep Chakladar, Lindsey Shallberg, Benjamin S. Waldman, Christopher
1005 A. Hunter, Sebastian Lourido. A positive feedback loop controls Toxoplasma chronic differentiation.
1006 Biorxvi. 2022.
1007 [67] Afroz T, Cienikova Z, Clery A, Allain FHT. One, Two, Three, Four! How Multiple RRMs Read the
1008 Genome Sequence. Methods in enzymology. 2015;558:235-78.
1009 [68] Malumbres M. Cyclin-dependent kinases. Genome biology. 2014;15:122.
1010 [69] Jin C, Zang C, Wei G, Cui K, Peng W, Zhao K, et al. H3.3/H2A.Z double variant-containing
1011 nucleosomes mark 'nucleosome-free regions' of active promoters and other regulatory regions.
1012 Nature genetics. 2009;41:941-5.
1013 [70] Colino-Sanguino Y, Cornett EM, Moulder D, Smith GC, Hrit J, Cordeiro-Spinetti E, et al. A
1014 Read/Write Mechanism Connects p300 Bromodomain Function to H2A.Z Acetylation. iScience.
1015 2019;21:773-88.
1016 [71] Rahal R, Amon A. Mitotic CDKs control the metaphase-anaphase transition and trigger spindle
1017 elongation. Genes & development. 2008;22:1534-48.
1018 [72] Lukasik P, Zaluski M, Gutowska I. Cyclin-Dependent Kinases (CDK) and Their Role in Diseases
1019 Development-Review. International journal of molecular sciences. 2021;22.
1020 [73] Ors A, Papin C, Favier B, Roulland Y, Dalkara D, Ozturk M, et al. Histone H3.3 regulates mitotic
1021 progression in mouse embryonic fibroblasts. Biochemistry and cell biology = Biochimie et biologie
1022 cellulaire. 2017;95:491-9.
1023 [74] Page MJ, Di Cera E. Evolution of peptidase diversity. J Biol Chem. 2008;283:30010-4.
1024 [75] Harvey SH, Krien MJ, O'Connell MJ. Structural maintenance of chromosomes (SMC) proteins, a
1025 family of conserved ATPases. Genome biology. 2002;3:REVIEWS3003.
1026 [76] Laflamme G, Tremblay-Boudreault T, Roy MA, Andersen P, Bonneil E, Atchia K, et al. Structural
1027 maintenance of chromosome (SMC) proteins link microtubule stability to genome integrity. J Biol
1028 Chem. 2014;289:27418-31.

1029 [77] Serrano D, Cordero G, Kawamura R, Sverzhinsky A, Sarker M, Roy S, et al. The Smc5/6 Core
1030 Complex Is a Structure-Specific DNA Binding and Compacting Machine. Mol Cell. 2020;80:1025-38
1031 e5.
1032 [78] Borgogno MV, Monti MR, Zhao W, Sung P, Argarana CE, Pezza RJ. Tolerance of DNA Mismatches
1033 in Dmc1 Recombinase-mediated DNA Strand Exchange. J Biol Chem. 2016;291:4928-38.
1034 [79] Kloehn J, Oppenheim RD, Siddiqui G, De Bock PJ, Kumar Dogga S, Coute Y, et al. Multi-omics
1035 analysis delineates the distinct functions of sub-cellular acetyl-CoA pools in Toxoplasma gondii. BMC
1036 Biol. 2020;18:67.
1037 [80] Attar N, Campos OA, Vogelauer M, Cheng C, Xue Y, Schmollinger S, et al. The histone H3-H4
1038 tetramer is a copper reductase enzyme. Science. 2020;369:59-64.
1039 [81] Singh A, Verma S, Modak SB, Chaturvedi MM, Purohit JS. Extra-nuclear histones: origin,
1040 significance and perspectives. Mol Cell Biochem. 2022;477:507-24.
1041 [82] Choi YS, Hoon Jeong J, Min HK, Jung HJ, Hwang D, Lee SW, et al. Shot-gun proteomic analysis of
1042 mitochondrial D-loop DNA binding proteins: identification of mitochondrial histones. Molecular
1043 bioSystems. 2011;7:1523-36.
1044 [83] Zanin MK, Donohue JM, Everitt BA. Evidence that core histone H3 is targeted to the
1045 mitochondria in Brassica oleracea. Cell Biol Int. 2010;34:997-1003.
1046 [84] Roson JN, Vitarelli MO, Costa-Silva HM, Pereira KS, Pires DDS, Lopes LS, et al. H2B.V demarcates
1047 divergent strand-switch regions, some tDNA loci, and genome compartments in Trypanosoma cruzi
1048 and affects parasite differentiation and host cell invasion. PLoS pathogens. 2022;18:e1009694.
1049 [85] Denkers EY, Gazzinelli RT. Regulation and function of T-cell-mediated immunity during
1050 Toxoplasma gondii infection. Clin Microbiol Rev. 1998;11:569-88.
1051 [86] Blader IJ, Saeij JP. Communication between Toxoplasma gondii and its host: impact on parasite
1052 growth, development, immune evasion, and virulence. APMIS. 2009;117:458-76.
1053 [87] Elsaid MM, Vitor RW, Frezard FJ, Martins MS. Protection against toxoplasmosis in mice
1054 immunized with different antigens of Toxoplasma gondii incorporated into liposomes. Mem Inst
1055 Oswaldo Cruz. 1999;94:485-90.
1056 [88] Sanchez-Lopez EF, Corigliano MG, Oliferuk S, Ramos-Duarte VA, Rivera M, Mendoza-Morales
1057 LF, et al. Oral Immunization With a Plant HSP90-SAG1 Fusion Protein Produced in Tobacco Elicits
1058 Strong Immune Responses and Reduces Cyst Number and Clinical Signs of Toxoplasmosis in Mice.
1059 Front Plant Sci. 2021;12:726910.
1060 [89] Buxton D, Innes EA. A commercial vaccine for ovine toxoplasmosis. Parasitology. 1995;110
1061 Suppl:S11-6.
1062 [90] Wu M, Liu S, Chen Y, Liu D, An R, Cai H, et al. Live-attenuated ME49Deltacdpk3 strain of
1063 Toxoplasma gondii protects against acute and chronic toxoplasmosis. NPJ Vaccines. 2022;7:98.
1064 [91] Echeverria PC, Matrajt M, Harb OS, Zappia MP, Costas MA, Roos DS, et al. Toxoplasma gondii
1065 Hsp90 is a potential drug target whose expression and subcellular localization are developmentally
1066 regulated. J Mol Biol. 2005;350:723-34.
1067 [92] Guzman F, Gauna A, Roman T, Luna O, Alvarez C, Pareja-Barrueto C, et al. Tea Bags for Fmoc
1068 Solid-Phase Peptide Synthesis: An Example of Circular Economy. Molecules. 2021;26.
1069 [93] Spiess PC, Deng B, Hondal RJ, Matthews DE, van der Vliet A. Proteomic profiling of acrolein
1070 adducts in human lung epithelial cells. J Proteomics. 2011;74:2380-94.

1071